

# Distribution-based pooling for combination and multi-model bias correction of climate simulations

Mathieu Vrac<sup>1</sup>, Denis Allard<sup>2</sup>, Grégoire Mariéthoz<sup>3</sup>, Soulivanh Thao<sup>1</sup>, and Lucas Schmutz<sup>3</sup>

<sup>1</sup>Laboratoire des Sciences du Climat et de l'Environnement (LSCE-IPSL), CEA/CNRS/UVSQ, Université Paris-Saclay, Centre d'Etudes de Saclay, Orme des Merisiers, 91191 Gif-sur-Yvette, France

<sup>2</sup>Biostatistics and Spatial Processes (BioSP), INRAE, Avignon 84914, France

<sup>3</sup>University of Lausanne, Institute of Earth Surface Dynamics (IDYST), UNIL-Mouline, Geopolis, 1015 Lausanne, Switzerland

**Correspondence:** Mathieu Vrac (mathieu.vrac@lsce.ipsl.fr)

**Abstract.** For investigating, assessing and anticipating climate change, tens of Global Climate Models (GCM)s have been designed, each modeling the Earth system slightly differently. To extract a robust signal from the diverse simulations and outputs, models are typically gathered into multi-model ensembles (MMEs). Those are then summarised in various ways, including (possibly weighted) multi-model means, medians or quantiles. In this work, we introduce a new probability aggregation method termed “alpha-pooling” which builds an aggregated Cumulative Distribution Function (CDF) designed to be closer to a reference CDF over the calibration (historical) period. The aggregated CDFs can then be used to perform bias adjustment of the raw climate simulations, hence performing a “multi-model bias correction”. In practice, each CDF is first transformed according to a non-linear transformation that depends on a parameter  $\alpha$ . Then, a weight is assigned to each transformed CDF. This weight is an increasing function of the CDF closeness to the reference transformed CDF. Key to the  $\alpha$ -pooling is a parameter  $\alpha$  that describes the type of transformation, and hence the type of aggregation, generalising both linear and log-linear pooling methods. We first establish that  $\alpha$ -pooling is a proper aggregation method verifying some optimal properties. Then, focusing on climate models simulations of temperature and precipitation over Western Europe, several experiments are run in order to assess the performance of  $\alpha$ -pooling against methods currently available, including multi-model means and weighted variants. A reanalyses-based evaluation as well as a perfect model experiment and a sensitivity analysis to the set of climate models are run. Our findings demonstrate the superiority of the proposed pooling method, indicating that  $\alpha$ -pooling presents a potent way to combine GCMs' CDFs. The results of this study also show that our unique concept of CDFs pooling strategy for “multi-model bias correction” is a credible alternative to usual GCM-by-GCM bias correction methods, by allowing to handle and consider several climate models at once.

## 1 Introduction

Over the past century, the Earth's climate has been undergoing significant warming, with the rate of this change accelerating notably in the past six decades (IPCC, 2023; Wuebbles et al., 2017). Such a warming is believed to be a catalyst not only for

extreme events, but also for an alteration in societal and economic systems (Stott, 2016; Wuebbles et al., 2017). In this context, Global Climate Models (GCMs) are seen as critical tools to simulate the future of our climate under different emissions scenarios and provide the scientific community and policy makers with essential climate information to guide adaptation to upcoming climatic changes (e.g., Arias et al., 2021; Eyring et al., 2016; Intergovernmental Panel on Climate Change (IPCC), 2014).

In recent years, tens of GCMs have been designed, modelling the physical processes in the atmosphere, ocean, cryosphere and land surface of the planet Earth differently, often by incorporating varied or uniquely modelled parameters (Eyring et al., 2016). However, the complexity of the processes represented means that these models are inevitably imperfect. They contain biases, meaning that, even over the historical period, they can fail to reproduce some statistics of the observed climate (e.g., François et al., 2020). To alleviate such errors, two distinct types of post-processing are typically applied to the models: bias correction and model combination. Bias correction methods aim at applying statistical corrections to climate model outputs, which can be as simple as a delta-change (Xu, 1999) or a “simple scaling” of variance (e.g., Eden et al., 2012; Schmidli et al., 2006), or as advanced as multivariate methods adjusting dependencies (e.g., François et al., 2020) such as based on multivariate rank resampling (Vrac, 2018; Vrac and Thao, 2020) or machine learning techniques (e.g., François et al., 2021). Model combination aims to extract a robust signal from the diversity of existing GCM outputs. Models are typically gathered into multi-model ensembles (MMEs), which are synthesised into multi-model means (MMMs). This approach is grounded in the belief that members of the MMEs are “truth-centered”. In other words, the various models act as independent samples from a distribution that gravitates around the truth, and as the ensemble expands, the MMM is expected to approach the truth (Ribes et al., 2017; Fragoso et al., 2018). The challenge of combining models lies not only in their inherent differences but also in the construction of the MME itself. While equal weighting of models is a common practice (e.g., Weigel et al., 2010), it does not account for possible redundancy of information between models. Indeed, climate models often share foundational assumptions, parameterizations, and codes, making their outputs redundant (Abramowitz et al., 2019; Knutti et al., 2017; Rougier et al., 2013). As a result, consensus among models does not necessarily result in reliable simulations. Advanced methods, such as Bayesian Model Averaging (Bhat et al., 2011; Kleiber et al., 2011; Olson et al., 2016) or Weighted Ensemble Averaging (Strobach and Bel, 2020; Wanders and Wood, 2016), have been developed to refine model weights. However, Bukovsky et al. (2019) found that the weighting approach does not substantially change the multi-model mean (i.e., MMM) results.

Furthermore, the usual model combination approach is to apply a global weighting of the models, which can dilute the accuracy of regional predictions. For instance, a model that accurately represents European temperatures might be deemed subpar overall, thus not contributing significantly to the European temperature projection in the ensemble. This could result in a global weighting approach that inaccurately represents this region. To address this, some studies have adopted a regional focus, selecting an optimal set of models for specific regions (Ahmed et al., 2019; Brunner et al., 2020; Dembélé et al., 2020; Sanderson et al., 2017). Yet, such strategies are still sub-optimal since they are only valid for a given study area, often of rectangular shape, and thus specific to the use case they have been developed for. Moreover, by construction, traditional model averaging techniques tend to homogenise the spatial patterns that are present in individual models, even though these patterns often stem

from genuine physical processes. Approaches that consider per-grid point model combinations have shown promise in enhancing performances in weather forecasting (Thorarinsdottir and Gneiting, 2010; Kleiber et al., 2011). Geostatistical methods, in particular, offer tools to characterise spatial structures and dependencies, providing a more nuanced approach to ensemble predictions (Gneiting and Katzfuss, 2014; Sain and Cressie, 2007). Recently, Thao et al. (2022) introduced a method that uses  
60 a graph cut technique stemming from computer vision (Kwatra et al., 2003) to combine climate models’ outputs on a grid-point basis. This approach aims to minimise biases and maintain local spatial dependencies, producing a cohesive “patchwork” of the most accurate models while preserving spatial consistency. However, one limit of the graph cut approach is that it only selects one single optimal model per grid point, whereas locally weighted averages of models might enable more subtle combinations that capitalise on the strengths of the ensemble of GCMs.

65 In addition, one limitation of all aforementioned model combination approaches is that they are all based on combining scalar quantities such as for example the decadal mean temperature produced by an ensemble of models. However, climate models’ outputs are much richer than averages. They typically produce hourly or daily climate variables, from which entire probability distributions can be derived. It therefore makes intuitive sense to combine distributions, such as to obtain an aggregated distribution that can borrow the most relevant aspects of all members of the MME. In statistics, the combination of distribu-  
70 tions, or probability aggregation, has been studied for applications in decision science and information fusion. Comprehensive overviews of the different ways of aggregating probabilities, and the hypotheses underlying each of them, are provided in Allard et al. (2012) and Koliander et al. (2022), notably based on the foundational works of Bordley (1982) .

In this study, we introduce an innovative probability aggregation method termed  $\alpha$ -pooling, which we apply to combine climate projections coming from several GCMs. It builds an aggregated Cumulative Distribution Function (CDF) designed to be as  
75 close as possible to a reference CDF. During a calibration phase, an optimization procedure determines the parameters characterising the transformation from a set of CDFs each representing a model, to a reference CDF. This transformation includes weights that increase with the closeness to the reference CDF, and a parameter  $\alpha$  that characterises how the transformation takes place. The optimization results in weights that are lower for models that are similar, i.e. that are redundant with each other. In that sense,  $\alpha$ -pooling combines models while addressing information redundancy. In addition, as  $\alpha$ -pooling provides  
80 an aggregated CDF close to a reference one, corresponding time series can be obtained, for example via quantile-quantile based techniques (e.g. Déqué, 2007; Gudmundsson et al., 2012) or its variants (e.g. Vrac et al., 2012; Cannon et al., 2015), hence providing bias corrected values of the combined model simulations. Therefore,  $\alpha$ -pooling not only combines model CDFs but also corrects biases between the CDF of each model and the reference CDF. So, we bring together, in an original way, “bias correction” and “model combination”, which are usually seen as different categories of methods, employed by separate scien-  
85 tific communities. We stress that our proposed  $\alpha$ -pooling method hinges on a unique concept that allows the simultaneous bias correction of multiple climate model simulations. This is accomplished through the innovative combination of model CDFs, which stands as an original concept in its own right.

Our application of the  $\alpha$ -pooling method focuses on the simultaneous combination and bias correction (BC) of climate models over Western Europe. Here, each member of the MME is perceived as an individual expert, whose Cumulative Distribu-

90 tion Function (CDF) is used in the combination. We compare  $\alpha$ -pooling with other model combination and bias correction techniques, including Multi-Model Mean (MMM), linear pooling, log-linear pooling, and CDF-transform (Vrac et al., 2012, CDFt.). Our analysis spans both short-term and extended projections of temperatures (T) and precipitation (PR), encompassed in three distinct experiments. In the first experiment, ERA5 serves as the reference, enabling performance evaluation against observational references. Subsequently, a perfect model experiment (PME) is employed, wherein each model is iteratively used  
95 as the reference. This PME approach offers insights into the stability of the alpha-pooling projections compared to other BC techniques, extending to the end of the century. A third experiment investigates the sensitivity of the aggregated CDFs to the choice of a specific subset of models to combine.

This paper is structured as follows. Section 2 describes the climate simulations and the reference used in this work. After some reminders on linear pooling and log-linear pooling, Section 3 presents the new  $\alpha$ -pooling. Section 4 describes the ex-  
100 periments carried out in this work and Section 5 describes the results obtained. In Section 6, we provide some conclusions and perspectives. Two appendices provide an approximate and faster alternative to the  $\alpha$ -pooling method as well as optimal properties.

## 2 Climate simulations and reference

The reference data used in this study are daily temperature (hereafter T) and precipitation (PR) time series extracted from the  
105 ERA5 daily reanalysis (Hersbach et al., 2020) over the 1981-2020 period, at a  $0.25^\circ$  horizontal spatial resolution. The Western Europe domain, defined as  $[10^\circ W, 30^\circ E] \times [30^\circ N, 70^\circ N]$ , is considered.

The same variables (T and PR) are also extracted for the period 1981–2100 from 12 Global Climate Models (GCMs) contributing to the 6<sup>th</sup> exercise of the “Coupled Models Intercomparison Project” (CMIP6, Eyring et al., 2016). This selection was dictated by the availability of T and PR fields at daily time scale at the time of analysis: we have only selected models whose  
110 data were fully available for the whole period 1981–2100. The list of used GCMs is provided in Table 1.

To ease the handling of the different simulated and reference datasets, all temperature and precipitation fields have been regrid-  
ded to a common spatial resolution of  $1^\circ \times 1^\circ$ . Moreover, for the sake of simplicity, in the following, we only consider winter — defined as December-January-February, DJF — and summer data — June-July-August, JJA — separately, to investigate and test our  $\alpha$ -pooling approach. Then, for each grid-point and each dataset, the univariate CDFs of temperature and precipitation  
115 are calculated. Here, empirical distributions are employed (i.e., step functions via the “ecdf” R function) in order not to fix the distribution family and thus let the data “speak for themselves”. Other parametric or non-parametric CDF modelling methods can be used if needed and appropriate.

Simulation name	Run	Atmospheric resolution	Data reference
* CNRM-CM6-1-HR	r1i1p1f2	~ 100 km	Voltaire (2019)
* GFDL-CM4	r1i1p1f1	~ 100 km	Held et al. (2019)
* IPSL-CM6A-LR	r14i1p1f1	~ 250 km	Boucher et al. (2018)
* MRI-ESM2-0	r1i1p1f1	~ 100 km	Yukimoto et al. (2019)
* UKESM1-0-LL	r1i1p1f2	~ 250 km	Tang et al. (2019)
BCC-CSM2-MR	r1i1p1f1	~ 100 km	Wu et al. (2018)
CanESM5	r10i1p1f1	~ 500 km	Swart et al. (2019)
INM-CM4-8	r1i1p1f1	~ 100 km	Volodin et al. (2019)
INM-CM5-0	r1i1p1f1	~ 100 km	Volodin et al. (2019)
MIROC6	r1i1p1f1	~ 250 km	Shiogama et al. (2019)
CESM2	r1i1p1f1	~ 100 km	Danabasoglu et al. (2020)
CESM2-WACCM	r1i1p1f1	~ 100 km	Danabasoglu et al. (2020)

**Table 1.** List of CMIP6 simulations used in this study, their run, approximate horizontal atmospheric resolution and references. The models preceded by a “\*” correspond to the 5 models used in the “ERA5 experiment” (sections 4.1 and 5.1) and the “Perfect Model Experiment” (sections 4.2 and 5.2). All 12 models are used in the “Sensitivity” experiment (sections 4.3 and 5.3). See text for details.

### 3 Combining models via the CDF-pooling approach

The CDF of a random variable  $X$  is the function  $F : \mathbb{R} \rightarrow [0, 1]$  defined as the probability that  $X$  is less than or equal to  $x$ , i.e.  $F(x) = P(X \leq x)$ . Combining CDFs amounts thus essentially to combine, or aggregate, probabilities for all values  $x$  in a way that makes the aggregated function a CDF, i.e. a non decreasing function with  $\lim_{x \rightarrow -\infty} F(x) = 0$  and  $\lim_{x \rightarrow \infty} F(x) = 1$ .

Allard et al. (2012) offers a review of probability aggregation methods in geoscience, with application in spatial statistics. Aggregation or pooling methods can be characterized according to their mathematical properties. Let us denote  $p_1, \dots, p_N$  the probabilities to be pooled together and  $p_G$  the resulting pooled probability. A pooling method verifying  $p_G = p$  when  $p_i = p$  for all  $i = 1, \dots, N$  is said to preserve unanimity. Furthermore, let us suppose that we are in the following case: there exists at least one index  $i$  such that  $p_i = 0$  (resp.  $p_i = 1$ ) with  $0 < p_j < 1$  for  $j \neq i$ . A pooling method which returns  $p_G = 0$  (resp.  $p_G = 1$ ) in this case is said to enforce a certainty effect, a property also called the *0/1 forcing property*. Notice that for a pooling method verifying this property, deadlock situations are possible, when  $p_i = 0$  and  $p_j = 1$  for  $j \neq i$ .

In the following, we will consider that there are  $N$  CDFs  $F_i(x)$ , with  $i = 1, \dots, N$ . Pooling methods must be applied simultaneously to all probabilities  $P(X \leq x) = F(x)$  and  $P(X > x) = 1 - F(x)$ . The aggregated (or pooled) CDF must verify all properties of a proper CDF recalled above.

### 3.1 Pre-processing: Standardising data

CDFs from climate model simulations can be very different from each other and from ERA5 CDFs. It is thus necessary to perform a preliminary standardization (i.e., basic adjustment) before pooling them. Note that the same operation is performed in many IPCC figures (WGI, 2021) when working on anomalies (instead of raw simulated or reference data). This allows easier comparison (and combination) of the different datasets. In the present study, temperature and precipitation are standardised differently. For temperature, the simulated data are rescaled such that the mean and standard deviation correspond to those of the reference data:

$$T_{rescaled} = \frac{T - m_{mod}}{\sigma_{mod}} \times \sigma_{ref} + m_{ref} \quad (1)$$

where  $m_{mod}$  and  $\sigma_{mod}$  are the mean and standard deviation of the model data to rescale, and  $m_{ref}$  and  $\sigma_{ref}$  are those from ERA5. For precipitation, the data are rescaled to get the 90% quantile similar to that of the reference precipitation:

$$PR_{rescaled} = PR \times Q90_{ref} / Q90_{mod} \quad (2)$$

where  $Q90_{ref}$  and  $Q90_{mod}$  are respectively the 90% quantiles from ERA5 and the model data to rescale. This choice of 90% is a trade-off that enables having a robust quantile estimation and also a sufficient spread in the range of precipitation values (Vrac et al., 2016).

In the rest of this paper, all tested pooling methods are then applied to standardized data. As a preliminary to our new  $\alpha$ -pooling approach, we first briefly present the linear and log-linear pooling with their main properties.

### 3.2 Linear pooling

The linear pooling, whose resulting pooled CDF is denoted  $F_L$ , is simply a weighted average of all CDFs:

$$F_L(x) = \sum_{i=1}^N w_i F_i(x), \quad \forall x \in \mathbb{R} \quad (3)$$

$F_L$  is a proper CDF if and only if all  $w_i$ s are non-negative and  $\sum_{i=1}^N w_i = 1$ . Note that with linear pooling, the probabilities are weighted for a given value  $x$ , which is quite different than averaging the quantiles for a given probability, as done in a usual weighted MMM (e.g., Markiewicz et al., 2020). Indeed, in our linear-pooling (3), the weighted average is performed on the CDFs (i.e., probabilities  $F_i(x)$ ) and not on quantiles (values) of the variable. While there is not an inherent problem with linear pooling, like any linear approach, the method may lack flexibility and thus fail to capture the necessary non-linearity required to adjust to the data and their CDF. That is why non-linear methods (e.g., log-linear pooling) have been developed.

### 3.3 Log-linear pooling

The log-linear pooled CDF, denoted  $F_{LL}$ , is found by considering that its logarithm is, up to a normalizing factor, a weighted average of the logarithm of the CDFs. Applying this to  $F(x)$  and  $1 - F(x)$  simultaneously, one gets:

$$160 \quad \ln F_{LL}(x) = K + \sum_{i=1}^N w_i \ln F_i(x), \text{ and } \ln(1 - F_{LL}(x)) = K + \sum_{i=1}^N w_i \ln(1 - F_i(x)),$$

where  $w_1, \dots, w_N$  is a set of  $N$  non-negative weights and  $K$  is the normalising factor. After some algebra, one finally obtains:

$$F_{LL}(x) = \frac{\prod_{i=1}^N F_i(x)^{w_i}}{\prod_{i=1}^N F_i(x)^{w_i} + \prod_{i=1}^N (1 - F_i(x))^{w_i}}, \quad \forall x \in \mathbb{R} \quad (4)$$

which is a proper CDF for all non-negative weights  $w_i$ . The condition  $S = \sum_{i=1}^N w_i = 1$  entails unanimity. On simulations, Allard et al. (2012) showed that log-linear pooling of probabilities leads consistently to the best validation scores among all  
 165 other tested pooling methods. However, log-linear pooling verifies the 0/1 forcing property. This is not necessarily a desirable property since  $F_{LL}$  belongs to the interval  $(0, 1)$  only for the restricted set of values  $x$  such that  $0 < F_i(x) < 1$  for all  $i = 1, \dots, N$ . Moreover,  $F_{LL}$  is undefined as soon as there exists a pair  $i, j$  with  $i \neq j$  such that  $F_i(x) = 0$  and  $F_j(x) = 1$ .

### 3.4 $\alpha$ -Pooling

In order to mitigate the problems faced with the log-linear pooling and the lack of flexibility of the linear pooling, we propose  
 170  $\alpha$ -pooling. Its theoretical expression is presented here. How the parameters are estimated from the models and the reference is shown in the next section. Our approach builds on the  $A_{\alpha-IT}$  transformation proposed in Clarotto et al. (2022), which uses the less stringent power transformation instead of the log transformation used in the log-linear pooling approach. We first recall briefly that a  $D$ -part composition is a vector  $(v_1, \dots, v_D)^t$  of  $D$  non-negative values such that  $\sum_{i=1}^D v_i = \kappa$  where  $\kappa$  is an arbitrary positive constant which can be set equal to 1 without loss of generality. In all generality,  $A_{\alpha-IT}$  transforms a  
 175 compositions with  $D$  parts (constrained to belong to the simplex of dimension  $D - 1$ ) to a vector with  $D - 1$  unconstrained and well-defined coordinates, even when some parts are equal to 0 (Clarotto et al., 2022). For all  $x \in \mathbb{R}$ , the vector  $\mathbf{F}(x) = (F(x), 1 - F(x))^t$  can be seen as a 2-part composition. In this case, the  $A_{\alpha-IT}$  transformation of  $\mathbf{F}(x)$  results in a scalar:

$$z(x) = A_{\alpha-IT}(\mathbf{F}(x)) = \alpha^{-1} \mathbf{H}_2 \mathbf{F}(x)^\alpha, \quad (5)$$

where  $\mathbf{H}_2$  is the  $(1, 2)$  Helmert matrix  $(\sqrt{2}, -\sqrt{2})$ , and where  $\mathbf{F}(x)^\alpha$  is the vector  $(F(x)^\alpha, (1 - F(x))^\alpha)^t$  with  $\alpha > 0$ . The  
 180  $\alpha$ -pooling postulates a linear aggregation of the scores  $z_i(x)$  with

$$z_G(x) = \sum_{i=1}^N w_i z_i(x) = \frac{\sqrt{2}}{\alpha} \sum_{i=1}^N w_i (F_i(x)^\alpha - (1 - F_i(x))^\alpha), \quad (6)$$

where, as above,  $w_1, \dots, w_N$  is a set of  $N$  non-negative weights summing to one, i.e. with  $\sum_{i=1}^N w_i = 1$ . The  $\alpha$ -pooling aggregated CDF  $F_G$  is thus the CDF such that  $z_G(x) = \frac{\sqrt{2}}{\alpha} (F_G(x)^\alpha - (1 - F_G(x))^\alpha)$ . Hence, for each  $x$ ,  $F_G(x)$  solves

$$F_G(x)^\alpha - (1 - F_G(x))^\alpha = \alpha z_G(x) = \sum_{i=1}^N w_i (F_i(x)^\alpha - (1 - F_i(x))^\alpha). \quad (7)$$

185 Let us define the function

$$G(y) = \alpha^{-1} [y^\alpha - (1 - y)^\alpha] \quad (8)$$

with  $0 \leq y \leq 1$ .  $G(y)$  is an increasing one-to-one function on  $[0, 1]$ , with  $G(0) = -\alpha^{-1}$ ,  $G(1/2) = 0$  and  $G(1) = \alpha^{-1}$ . One thus gets  $F_G(x) = G^{-1}(z_G(x))$ , where  $G^{-1}$  is the inverse function of  $G$ , which exists and is unique. There is unfortunately no general closed form solution to (7) for all values of  $\alpha$  but the aggregated probability can be found as

$$190 \quad F_G(x) = G^{-1}(z_G(x)) = \arg \min_{y \in [0, 1]} (G(y) - z_G(x))^2 \quad (9)$$

using numerical optimisation. It is straightforward to check that when  $\alpha = 1$ , the solution to (7) is the linear pooling. Likewise, using  $\lim_{\alpha \rightarrow 0} F_i(x)^\alpha = 1 + \alpha \ln F_i(x)$ , it is easy to check that the  $\alpha$ -pooling tends to the log-linear pooling as  $\alpha \rightarrow 0$ . We can show the following:

**Proposition 1.** *The function  $F_G(x)$  defined in (7) and (9) is a proper CDF.*

195 **Proof:** The derivative of  $z_G(x)$  with respect to  $x$  is  $z_G(x)' = \sqrt{2} \sum_{i=1}^N w_i f_i(x) (F_i(x)^{\alpha-1} + (1 - F_i(x))^{\alpha-1}) \geq 0$ . Hence  $z_G(x)$  is a non decreasing function of  $x$ . Since the derivative of the function  $G(y)$  with respect to  $y$  is also positive, the function  $F_G(x) = G^{-1}(z_G(x))$  is increasing because it is the composition of two increasing functions. In addition, using that  $\lim_{x \rightarrow -\infty} F_i(x) = 0$  and  $\lim_{x \rightarrow \infty} F_i(x) = 1$  together with  $\sum_{i=1}^N w_i = 1$ , it is easy to check that  $\lim_{x \rightarrow -\infty} F_G(x) = 0$  and  $\lim_{x \rightarrow \infty} F_G(x) = 1$ . Hence,  $F_G$  is a proper CDF.  $\square$

200

The  $\alpha$ -pooling presented in (7) mitigates the principal inconvenient of the log-linear pooling, since it eliminates the 0/1 forcing property and it is well defined for all values of  $F_i(x)$ . In addition it accommodates seamlessly the case  $F_i(x) = 0$  and  $F_j(x) = 1$  with  $i \neq j$ .

**Remark 1.** *The constraint on the sum of the weights can be relaxed. In this case, if  $S = \sum_{i=1}^N w_i > 1$ ,  $F_G$  will still be a proper*  
 205 *CDF because  $y$  is constrained to belong to the interval  $[0, 1]$  in (9). But if  $S < 1$ , the lower and upper limits of  $F_G$  will not be equal to 0 and 1, respectively, with  $\lim_{x \rightarrow -\infty} F_G(x) = G^{-1}(-S/\alpha) = b > 0$  and  $\lim_{x \rightarrow \infty} F_G(x) = G^{-1}(S/\alpha) = 1 - b < 1$ .*

In Appendix A, we present a closed-form expression which is a very good approximate solution to (7) in most cases, i.e. except when  $S > 1$ . Then in appendix B, we present some optimal properties of the  $\alpha$ -pooling presented above related to the fact that  $\alpha$ -pooling derives from the general class of quasi-arithmetic pooling methods and corresponds to a proper scoring rule  
 210 (Neyman and Roughgarden, 2023).

An illustration is provided in Fig. 1(a) for  $N = 3$  distributions  $F_1$ ,  $F_2$  and  $F_3$  to be combined, corresponding respectively to a log-normal CDF, a Gaussian one and a Student t distribution. A Uniform CDF is arbitrarily fixed as reference. Despite the fact that they belong to very different families, the four CDFs are constructed here such that they have the same mean and variance, i.e., they respect the constraints of our real-case application (see Section 3.1). For this example, the estimated  $\alpha$  parameter tends



215 to 0 and  $w_1 = 0.06$ ,  $w_2 = 0.79$  and  $w_3 = 0$ . The higher value for  $w_2$  than for  $w_1$  or  $w_3$  indicates that the reference uniform CDF is closer to  $F_2$  (i.e., the Gaussian distribution) than to the others, which was expected considering the behaviour of  $F_1$  and  $F_3$  in the lower tail. Overall, given the difficulty of the illustration (very different CDFs), the  $\alpha$ -pooling pooled CDF (shown by the black dashed line in Fig. 1(a)) is able to approximate reasonably well the reference CDF (blue line), despite some larger errors on the upper tail. Notice that it performs significantly better than the linear pooling (red and green lines). In addition, 220 Fig. 1(b) displays the z-scores (i.e.,  $G$  in function of  $x$  in Eq. (8)) for the 3 CDFs to be combined, the reference one and the resulting  $\alpha$ -pooling CDF.

### 3.5 Estimating the parameters and computing the aggregated CDF

Given  $N$  CDFs  $F_i$ ,  $i = 1, \dots, N$  and a reference CDF  $F_0$ , the parameters are estimated by minimising the quadratic distance

$$Q = \sum_{k=1}^K (x_k - x_{k-1}) (F_0(x_k) - F_G(x_k))^2, \quad (10)$$

225 where  $F_G(x)$  is obtained by solving (7) and where  $x_0, \dots, x_K$  is an increasing sequence discretizing the real line. The ‘‘L-BFGS-B’’ optimisation algorithm (Byrd et al., 1995) is launched to minimise (10) and find the weights and the  $\alpha$  parameter. This algorithm is a limited-memory extension of the BFGS quasi-Newton method and allows to handle simple bound constraints on the variables. The parameter  $\alpha$  and the weights must be positive, and the weights can be constrained to sum to 1 or not. In the following, the sum  $S$  of weights is let free, i.e., not necessarily equal to one. Indeed, preliminary results indicated that 230 this freedom gives more flexibility to the  $\alpha$ -pooling and thus better aggregated CDFs (not shown). When unconstrained, it was found that in most cases the optimal sum  $S$  was close to one. There are two reasons for this: when  $S < 1$ , the pooled CDF varies from  $b$  to  $1 - b$  (see Remark 1). As a consequence,  $b$  must be as close to 0 as possible, and hence  $S$  as close to 1 as possible for the pooled CDF to be close to the reference; when  $S > 1$ , the inverse of all values  $z_G < -1/\alpha$  (resp. values  $z_G > 1/\alpha$ ) lead to the same inverse equal to 0 (resp. 1). A too high value of  $S$  is therefore likely to lead to a lack of fit in the lower and upper tails. 235 However, when  $S < 1$ , as the aggregated CDF goes from  $b > 0$  to  $1 - b < 1$ , it is not a proper CDF *per se*. Hence, a ‘‘min-max’’ rescaling of the aggregated CDF  $F_G$  is performed such that the rescaled CDF  $F_{resc}$  is always in  $[0, 1]$ :

$$F_{resc}(x) = \frac{F_G(x) - \min_x(F_G(x))}{\max_x(F_G(x)) - \min_x(F_G(x))} = \frac{F_G(x) - b}{(1 - b) - b} = \frac{F_G(x) - b}{1 - 2b} \quad (11)$$

In practice, this rescaling is only very slight as  $b$  is very often found extremely small, say less than  $10^{-3}$ .

The weights are easily interpretable since, as rule, the higher the weight  $w_i$ , the closer  $F_i$  is to the reference  $F_0$ . The parameter 240  $\alpha$  has a less immediate interpretation. As shown in Clarotto et al. (2022), the  $A_{\alpha-IT}$  transform can be seen as a difference between the Box-Cox transformation of  $F(x)$  and that of  $(1 - F(x))$  (see also Appendix A). The parameter  $\alpha$  can thus be interpreted as the power necessary to deform all CDFs (reference and models) in order to get an optimal linear pooling for these deformed CDFs, from log transform ( $\alpha \rightarrow 0$ ) to no transform ( $\alpha = 1$ ), to quadratic transform ( $\alpha = 2$ ), etc.

### 3.6 Benchmarking $\alpha$ -pooling: CDF-Multi-Model Mean (MMM) and linear pooling

245 As a benchmark for evaluating the  $\alpha$ -pooling approach, two CDF pooling methods are also applied. The first one is the simplest and consists in defining a “mean” CDF based on the  $N$  CDFs to be combined. Let us consider for example  $N = 2$  GCMs with respectively CDFs  $F_1$  and  $F_2$ , say of temperature, for a given grid-cell. For any temperature value  $x$ , the mean CDF  $F_{MMM}(x)$  corresponds to the average of  $F_1(x)$  and  $F_2(x)$ . An example is given in Fig. 1(a) for the three distributions used to illustrate the  $\alpha$ -pooling method. Here,  $F_{MMM}$  is shown as a red dashed line. Note that, for MMM, the reference CDF is not used at all, as  
250 the  $N$  CDFs are linearly averaged with weights all equal to  $1/N$ , whatever the quality of the different model CDFs with respect to that of the reanalysis. Hence, it is not surprising that  $\alpha$ -pooling approximates better the reference CDF over the calibration period.

The second CDF pooling method applied for comparison is the linear pooling described in Eq. (3). Here, contrary to MMM, the reference CDF is used to infer the weight parameters. By comparing the linear and  $\alpha$ -pooling methods, we can assess the  
255 potential added-value brought by the alpha parameter.

The same illustration as previously is also given in Fig. 1(a) for linear pooling, with the green dashed line. Based on this illustrative — but difficult — example, it is clear that the introduction of the  $\alpha$  parameter allows us to get closer to the reference CDF, at least over the calibration period. This is clear from the value of the L2 norm computed between the resulting CDF (i.e.,  $\alpha$ -pooling, linear-pooling or MMM) and the reference:  $\alpha$ -pooling has the smallest  $L^2$  (0.003), linear-pooling’s  $L^2$  is  
260 doubled (0.006), while it is almost tenfold for MMM (0.024). However, one major objective of this study is also to evaluate how MMM, linear pooling and  $\alpha$ -pooling behave in a projection period where climate changes occurs. When driven only by model CDFs over a projection (future) period, are the three pooling methods able to capture the changes in reference (temperature or precipitation) CDFs?

### 3.7 Bias corrections from CDF-pooling results

265 The aggregated CDF can be used within a CDF-based bias correction method applied to GCMs and, hence, to obtain corrected simulations in a way that preserves the temporal rank dynamics. Indeed, once  $\hat{F}$  is estimated over a projection period, one can apply a quantile-mapping technique (e.g., Gudmundsson et al., 2012, among many others) between  $\hat{F}$  and the CDF  $F_m$  of a given model  $m$  over the same period: for any value  $x$  simulated by model  $m$ , it consists in finding the value  $y$  such that  $\hat{F}(y) = F_m(x)$  which is equivalent to:

$$270 \quad y = \hat{F}^{-1}(F_m(x)) \quad (12)$$

where  $\hat{F}^{-1}$  is the inverse CDF function, allowing to compute the quantile associated to a given probability. Therefore, by applying Eq. (12) successively to all simulations from model  $m$ , we can obtain bias corrections. Those have the same rank chronology as that of model  $m$  but their values follow distribution  $\hat{F}$ . By applying this bias correction technique to the different models employed within the MMM, linear or  $\alpha$ -pooling methods, the  $N$  bias corrected time series have the exact same  
275 distribution (i.e.,  $\hat{F}$ ) but their temporal dynamics are different, as stemming from the  $N$  models.

### 3.8 “Model-by-model” bias correction via CDF-t

To evaluate the pros and cons of the bias corrections brought by the proposed pooling approaches, a more traditional “Model-by-model” bias correction method is also applied for comparison: the “Cumulative Distribution Function - transform” (CDF-t) method (Michelangeli et al., 2009; Vrac et al., 2012). It consists in a quantile-mapping technique (e.g., Panofsky and Brier, 1968; Haddad and Rosenfeld, 1997; Déqué, 2007; Gudmundsson et al., 2012) allowing to account for changes in the distributional properties of the climate simulations from the reference to the projection period. The reference CDF  $F_{Rp}$  over the projection period is first estimated as a composition of  $F_{Rc}$ ,  $F_{Mc}$  and  $F_{Mp}$ , respectively the reference CDF over the calibration period, the model CDF over the calibration period and the projection period:

$$\hat{F}_{Rp}(x) = F_{Rc}(F_{Mc}^{-1}(F_{Mp}(x))) \quad (13)$$

where  $F_{Mc}^{-1}$  is the inverse CDF function of  $F_{Mc}$ . See Vrac et al. (2012) or François et al. (2020) for more details. Based on the estimated projection reference CDF, a quantile-mapping is then fitted between  $\hat{F}_{Rp}$  and  $F_{Mp}$  to bias correct the simulations from the model  $M$ . Hence, in the case of  $N$  climate models to adjust,  $N$  CDF-t bias corrections are defined and applied.

## 4 Design of experiments

In the following, three experiments are described to evaluate and compare  $\alpha$ -pooling, linear pooling, MMM and CDF-t. For the sake of clarity and space, these experiments are carried out separately over two seasons only: winter (December, January, February – DJF) and summer (June, July, August – JJA). Only winter results are given in the following but summer results can be found as supplementary materials.

### 4.1 ERA5 experiment

The first experiment considers ERA5 reanalysis as reference. When considering linear and  $\alpha$ -pooling methods, for each grid-point and variable, we calibrate the approaches using  $N$  climate models with ERA5 data as reference over the calibration period 1981-2000. Then, we use the calibrated parameters ( $w_i$  and  $\alpha$ ) to combine the models CDFs over the projection period 2001-2020. For CDF-t, the same calibration period (1981-2000) is used, and the corrections are made for each model independently for the projection period (2001-2020). For MMM, the CDFs of the climate models are directly averaged over 2001-2020. The results of each approach are then compared to the ERA5 data over 2001-2020.

In this experiment, only 5 GCMs are used. This is partly constrained by the  $\alpha$ -pooling method that can have stability issues to infer the parameters when combining a large number of models. When a relatively high number of models (i.e., CDFs) are combined, such as 10, depending on the initialization values of the parameters in the inference algorithm, the “optimal” final parameters may vary. In essence, the optimized parameters are unstable in such a case. This is because many local minima attain undistinguishable L2 distances. Indeed, while final parameters may differ between initializations, the minimized criterion values – specifically, the quadratic distance in the CDF-space outlined in Eq. (10) – remain relatively consistent,

often converging to similar or nearly identical values. Although it has been tested with more than 10 models, the use of 5 GCMs appeared as a good compromise in the sense that (i) it ensured not only stability in the quadratic criterion but also consistency in the final optimized parameters, (ii) it allows a reasonable computation time (e.g., no more than a few minutes of computations for each location/variable), and (iii) it employs a sufficient number of simulations to get robust results. These 5 GCMs (indicated with “\*” in table 1) were selected on the basis of a preliminary analysis showing that they approximately represent the spread of future evolution of all 12 GCMs (not shown). Note that 4 models (IPSL-CM6A-LR, MRI-ESM2-0, UKESM1-0-LL, GFDL-CM4) out of the 5 selected ones are consistent with the choice made in the ISIMIP3 project (Lange and Büchner, 2021; Lange, 2021) for bias correction objectives.

The evaluations are performed in terms of biases of the obtained 2001-2020 temperature and precipitation with respect to ERA5. For each grid-point, dataset, variable, and season (winter or summer), some statistics  $T$  are calculated. For temperature, statistics include the mean, standard deviation and 99% quantile (Q99). For precipitation, we consider the conditional mean given a wet state (Cm), probability of dry day ( $P_1$ ) and the 99% quantile. A day with PR value lower than 1mm is considered as dry (and thus  $>1\text{mm}$  as wet).

Then, absolute biases are calculated as

$$B(m, T) = T(m) - T(\text{ERA5}) \quad (14)$$

for temperature mean and Q99, while relative biases are calculated as

$$B(m, T) = \frac{T(m) - T(\text{ERA5})}{T(\text{ERA5})} \quad (15)$$

for temperature standard deviation and precipitation conditional mean,  $P_1$  and Q99.  $m$  denotes the method ( $\alpha$ -pooling, linear-pooling, MMM or CDF-t) and  $T(X)$  is the statistics calculated from dataset  $X$  (ERA5 or method results).

## 325 4.2 Perfect Model Experiment (PME)

As the ERA5 experiment evaluates the methods on a projection period (2001-2020) very close to the calibration one (1981-2000), it does not allow understanding their quality in a strong climate change context. To perform such an assessment, we propose a “Perfect Model Experiment” (e.g. de Elía et al., 2002; Vrac et al., 2007; Krinner and Flanner, 2018; Robin and Vrac, 2021; Thao et al., 2022; Vrac et al., 2022, among many others). The main idea is that one model, among  $N$ , is taken as the reference. For the four methods, the procedure is the following:

- $\alpha$ -pooling and linear pooling are calibrated to combine the other  $N - 1$  models over 1981-2000. The obtained parameters (i.e.,  $w_i$  and  $\alpha$  for  $\alpha$ -pooling or  $w_i$  only for linear pooling) are next used to combine the  $N - 1$  models over five different future 20-year periods: 2001-2020; 2021-2040; 2041-2060; 2061-2080; 2081-2100.
- The same approach is followed for CDF-t: one model serves as reference over 1981-2000 to calibrate CDF-t – here separately for each of the  $N - 1$  remaining models – which is then used to bias-correct each model simulation over the five future periods.

- As previously for the ERA5 experiment, MMM does not require any calibration. CDF averaging is directly applied to combine the  $N - 1$  models for each of the five periods.

Over each future period and each grid-point, biases can then be evaluated with respect to the reference model. For temperature, it includes: absolute biases (Eq. (14)) of mean, 1% quantile, 99% quantile, minimum and maximum, as well as relative biases (Eq. (15)) of standard deviation. For precipitation, relative biases are computed for conditional mean given wet, probability of dry ( $< 1\text{mm}$ ) day, standard deviation, conditional 99% quantile given wet, unconditional 99% quantile, and maximum.

Hence, no observational or reanalysis data are used as reference in this experiment. Indeed, this PME is made under the “*models are statistically indistinguishable from the truth*” paradigm (e.g. Ribes et al., 2017), where “*the truth and the models are supposed to be generated from the same underlying probability distribution*” (Thao et al., 2022). Therefore, an evaluation framework based on this paradigm can consider any model as the reference. In practice in our PME, the same 5 models as in the ERA5 experiment (Section 4.1) are used and each model is used in turn as the reference. The four methods are thus tested on a diversity of possible references, encompassing cases where the truth can be either in the centre of the multi-model distribution or far in the tail.

### 350 4.3 Sensitivity of projected future CDFs to the choice of models

Finally, our third experiment aims to evaluate the uncertainty brought by the choice of the  $N$  models to combine and/or bias-correct. If this sensitivity is not much present over the calibration period – by construction, linear pooling,  $\alpha$ -pooling and CDF-t are relatively close to the reference CDFs over this period – or over periods very close to the calibration, the results of the four methods applied to long-term future projections can be sensitive to the chosen  $N$  models. To evaluate this sensitivity, for each variable, linear pooling,  $\alpha$ -pooling and CDF-t are calibrated with respect to ERA5 data over 1981-2000. Then, all methods are applied to 2081-2100 projections. However, in this experiment, linear pooling,  $\alpha$ -pooling and MMM do not combine a unique set of 5 models (as in the ERA5 experiment). Instead, 100 different sets of  $N=5$  models among the 12 presented in Table 1 are randomly drawn. The resulting 100 samples have been checked to contain each model in a uniform proportion (not shown). The linear pooling,  $\alpha$ -pooling and MMM methods are then applied 100 times, each with 5 models to combine, while CDF-t is applied to the 12 models separately. The 2081-2100 results obtained from each method and set of models do not allow any evaluation per se, as there is no reference over the future period. However, the use of multiple sets of models allows quantifying and comparing the statistical uncertainty brought by the choice of models, for each method. In this experiment, for both temperature and precipitation, only 6 grid-points are considered, corresponding to major capitals of the geographical domain: Paris (France), London (UK), Rome (Italy), Madrid (Spain), Berlin (Germany), Stockholm (Sweden).

### 5.1 ERA5 experiment results

Before looking at the results of the ERA5 experiment, it is interesting to visually understand how the  $\alpha$ -pooling parameters are spatially distributed over the geographical domain. Hence, Figure 2 displays maps of the winter (2.a and c) and summer (2.b and d) for the  $\alpha$  parameter, for temperature (2.a and b) and precipitation (2.c and d). First, note that the range of  $\alpha$  is not the same for T and PR. While for temperature most of the values are lower than 1 (no unit), the range goes up to 2.5 for precipitation. Moreover, for both seasons, more pronounced spatial structures appear for T than for PR, the latter  $\alpha$  maps appearing more “pixelated”. This can be explained by the widely recognized spatial variability of precipitation, encompassing both occurrence and intensity, which is often challenging to accurately capture in climate models and thus reflected in the spatial diversity in the estimated alpha-pooling parameters. However, globally, even for PR, large regions share similar  $\alpha$  values, indicating some spatial consistency of the parameters.

Regarding the weights parameters of  $\alpha$ -pooling, winter maps are provided in Figures 3 and 4 for temperature and precipitation respectively. The results for summer are given as supplementary information in Figures S1 and S2. The spatial structures of the weights are clearly visible (for both T and PR) and even more pronounced than for the  $\alpha$  maps. This strongly indicates that  $\alpha$ -pooling identifies large zones where some models have a larger influence on the combination and, thus, whose CDFs are closer to that of ERA5. Note however that for both variables, none of the models has the highest weights for all grid-points of the domain. In other words, over this European region, each of the 5 models brings some valuable contribution, although contrasted depending on the sub-region. For example with temperature, UKESM (panel 3.e) shows the strongest contributions over the Mediterranean sea, while MRI-ESM2 (panel 3.d) displays the largest weights over the northeast part of the domain. Interestingly, the spatial distributions of the weights are not the same for T and PR. Thus, there is no clear link between the contribution of each variable, confirming that results from one variable cannot be generalised to another.

A concentration index is displayed in panels (f) of Figures 3 and 4, which is equal to the sum of the squares of the 5 normalized weights. It takes the value 1 when one single GCM takes all the weight and reaches a minimum of  $1/N = 0.2$  when the 5 normalized weights are equally distributed. The concentration index can only be applied to weights summing to one. In our implementation of  $\alpha$ -pooling, the sum of weights is let free and, thus, not constrained to one. Although this sum remains quite close to 1 (mostly between 0.95 and 1.05 for temperature and between 0.92 and 1.1 for precipitation, not shown), normalization is required, which is accomplished by dividing the weights by  $S = \sum_{i=1}^N w_i$  before computing the concentration index. For temperature, panel 3.f) shows relatively well distributed weights (most concentration indices between 0.2 and 0.7) despite two zones (close to Italy and close to Greece) strongly influenced by one single GCM (UKESM1, see panel 3.e). For precipitation, more zones show the concentration index close to one: for example, the northwestern part of the domain and northern France (MRI-ESM2, panel 4.f), south Norway and northeastern part of the domain (CNRM-CM6, 4.a), or eastern Adriatic coast (UKESM1, 3.e). Note also that the maps of weights obtained from linear pooling are given in supplementary material as figures S3 and S4 for temperature and S5 and S6 for precipitation. Interestingly, the spatial structures of the weights and

concentration indices are very similar to those from  $\alpha$ -pooling. This confirms that the  $\alpha$  parameter does not modify structurally the interpretation of the weights but brings additional flexibility.

400 The biases of the different methods with respect to 2001-2020 ERA5 are shown in terms of mean, standard deviation and Q99 for winter temperature in Fig. 5 and in terms of conditional mean given wet, probability of dry day ( $P_1$ ) and Q99 for winter precipitation in Fig. 6. The equivalent figures for summer are provided as supplementary material in Figures S7 and S8 for temperature and precipitation respectively. In these figures, the columns are associated with the different biases. The top row shows maps of biases for MMM, row 2 for  $\alpha$ -pooling, row 3 for CDF-t and fourth row for linear-pooling. Note that, because  
405 CDF-t is applied separately for each GCM, the third row corresponds to the grid-point median of the CDF-t biases. The fifth (bottom) row displays a more condensed view of the results via boxplots of biases.

For temperature (Fig. 5), the differences between the maps of biases from the four methods are not very pronounced. This is especially true for the biases in mean temperature and standard deviation (sd). Some more differences appear for Q99. For instance, MMM (panel 5.c) shows relatively high positive bias ( $\sim 4^\circ C$ ) over the Northeastern part of the domain (Sweden and  
410 Finland), while biases for  $\alpha$ -pooling Q99 (panel 5.f), CDF-t (median) (panel 5.i) and linear pooling (panel 5.l) do not present this structure. Also, CDF-t median Q99 (panel 5.i) have a positive ( $\sim 1 - 2^\circ C$ ) bias pattern over the central domain (Germany, Italy, Poland, Hungary, Romania) while the three other methods show more nuanced and mixed structures. When looking at the more integrated boxplots view (bottom row in Fig. 5), the similar behaviour of  $\alpha$ -pooling, linear-pooling and MMM is visible for the three biases: the boxplots are relatively equivalent from one method to another. However, even though this is also the  
415 case for the CDF-t median biases – at least for mean and sd, and to some extent for Q99 –, the individual CDF-t biases (i.e., GCM by GCM) show a much larger variability, indicating that relying on a single GCM to perform the bias correction might lead to stronger errors within this ERA5 experiment.

For precipitation (Figure 6), conclusions are somewhat similar, but some more differences between methods are now more visible. For example, on the Norwegian sea, the relative biases of  $P_1$  for MMM (Fig. 6.b) have a large and strongly positive  
420 structure ( $\sim 1$ ) that does not appear in the other methods. Another example is the mostly negative bias ( $\sim -1$ ) in  $\alpha$ -pooling Q99 (6.f) over the North-African part of the domain, while MMM and (median) CDF-t show mostly highly positive biases and linear pooling more mixed patterns for this region. The boxplots view for winter precipitation is similar to that for temperature: roughly equivalent boxplots for the four methods, with more variability from the individual CDF-t results.

Note, however, that the ERA5 experiment results for summer (Figures S7 and S8 of the supplementary material) show more  
425 differences between the four methods – especially in the boxplots –, slightly in favour of the linear and  $\alpha$ -pooling methods, which show boxplots more centered around 0 for all biases and variables.

In the ERA5 experiment, the results are relatively similar for the four methods. This indicates that the added flexibility provided by  $\alpha$ -pooling may not be required over the 1981-2020 period of ERA5. This can nevertheless be different when considering other projection periods and reference datasets. Furthermore, the evaluation (2001-2020) and calibration (1981-2000) periods  
430 are quite close to each other, resulting in similar outcomes for both periods. These two results suggest that distinguishing be-

tween the different methods may be challenging in a climate that is relatively stable or undergoing minimal change. However, our primary objective is to assess and compare our various pooling strategies in the context of a significant climate change. Given that climate changes (in temperature and precipitation) from 1980 to 2100 in the SSP8.5 CMIP6 simulations are significantly more pronounced than what can be seen in the whole ERA5 reanalysis dataset over western Europe, the “perfect model  
435 experiment” (PME) will effectively and more clearly fulfill this purpose.

## 5.2 PME results

PME is first applied here to winter temperature, and summer results are in supplementary material. For each period and method, the boxplots of the different biases, computed at each grid point, are provided in Figure 7 (PME summer temperatures are in Fig. S9). As expected, for all biases, the more distant the period, the larger the boxplots, indicating an increase in possible  
440 statistical errors for periods further in the future. For brevity, we now focus on the last period (i.e. p6, 2081-2100), which results in the most pronounced differences between methods. For mean T bias (7.a), all four approaches show similar performance, although CDF-t has a wider boxplot. The bias of minimum temperature (7.e) is roughly equivalent for MMM and the linear- or  $\alpha$ -pooling approaches, while CDF-t presents, on average, a negative bias. However,  $\alpha$ -pooling appears slightly better than  
445 equivalent to  $\alpha$ -pooling but with a larger variability. For maximum temperature (7.f), CDF-t shows a strongly positive bias, while its biases look reasonable – at least more comparable to the other methods – for standard deviation (7.b) and 99% quantile (Q99, 7.d). Globally, for temperature standard deviation (7.b), Q99 (7.d) and maximum value (7.f),  $\alpha$ -pooling is more robust than the other methods since it clearly provides smaller biases over the 2081-2100 period.

Figure 8 shows the PME results for winter precipitation (summer results in Fig. S10). As was the case for temperature, the more  
450 distant the period, the wider the boxplots, although this is less pronounced here. Over 2081-2100, CDF-t results are often the most biased, except for the probability of dry day ( $P_1$ , 8.b) where it is as good as the other methods. As in Fig. 7.f, the maximum values of precipitation from CDF-t (green boxplot in Figure 8.f) show strong biases with a high variability. Regarding MMM, linear- and  $\alpha$ -pooling methods, they give about similar biases in terms of conditional mean precipitation given wet ( $C_m$ , 8.a) and  $P - 1$  (8.b) but more differences are visible for all other types of bias in favour of  $\alpha$ -pooling. Indeed, for precipitation  
455 standard deviation(8.c), condition 99% quantile (CQ99, 8.d), unconditional 99% quantile (Q99, 8.e) and maximum value (8.f), the  $\alpha$ -pooling biases (blue boxplots) are always more centred around 0 and with a smaller variability than the linear pooling and MMM biases.

The results from this PME experiment allow us to conclude that the proposed  $\alpha$ -pooling method is robust in a climate change context, for both temperature and precipitation. In addition, it also indicates that a bias correction technique based on an MMM  
460 (i.e., averaging) or linear combination of the GCM CDFs can be useful and robust, although the best results are achieved by the  $\alpha$ -pooling technique.



### 5.3 Sensitivity experiment results

The conclusions brought by the perfect model experiment are based on the pooling and bias correction of 5 climate models, somewhat arbitrarily selected. One can wonder about the uncertainty or sensitivity of the resulting projected (i.e., future) CDFs of T and PR if other climate models were selected. This is the reason why we perform the sensitivity experiment detailed in section 4.3.

For each of the 6 selected cities over 2081-2100, Figure 9 shows the 75% confidence envelope of the 100 winter temperature CDFs obtained from MMM (red lines),  $\alpha$ -pooling (blue lines) and linear-pooling (light blue lines), as well as the 75% envelope from the 12 CDF-t results (green lines). Figure 10 show the 75% confidence envelopes for winter precipitation CDFs. Summer CDF results are given in Figures S11 and S12.

All temperature corrections show a shift of the CDFs towards higher values, for all 6 cities. All combination approaches (i.e., MMM, linear- and  $\alpha$ -pooling) have very similar 75% envelopes for Paris (9.a) and relatively close for Berlin (9.e) and Stockholm (9.f). The other cities present some more differences. The three combination-based methods show similar lower bounds for London but with a higher upper bound for the linear- and  $\alpha$ -pooling techniques (depending on the quantiles). Rome and Madrid have an MMM envelope shifted towards lower temperature with respect to the other methods. CDF-t 75% envelopes are generally larger and thus comprise most of the envelopes

for any of the 6 cities. For precipitation (Fig. 10), as expected, the future projections – and thus their corrections – show varying trends depending on the cities. The combination-based methods give 75% CDF envelopes showing more rain in Paris, London, Berlin and, to some extent, Stockholm (10.a, b, e, f), while they result in less rain in Rome (10.c). Madrid (10.d) appears as the most uncertain for linear and  $\alpha$ -pooling – whose CDF envelope contains the ERA5 precipitation CDF –, while MMM shows more frequent low to medium rain but less frequent heavy rain. For most cities, CDF-t envelopes tend to have lower bounds showing a potential negative shift of the precipitation CDFs with respect to ERA5.

In addition to the position of these envelopes, their size is also important. Hence, the widths of the 75% CDF confidence envelopes for the 6 cities over 2081-2100 in winter are given in Figure 11 for temperature and Figure 12 for precipitation. For temperature, it is clear that CDF-t has, by far, the largest envelopes widths, while MMM has generally the smallest ones. It was somewhat expected that the linear- and  $\alpha$ -pooling have a larger uncertainty than MMM. Indeed, the use of weights means that models with higher weights will have a stronger influence on the resulting CDFs and bias corrections. Thus, even if these models do not closely align with reality during the projection period, their influence can lead to combined projections that can significantly deviate from the simple average performed by MMM. However, there is no such a systematic conclusion for precipitation, showing much more variable rankings, depending on the cities and on the probability values.

Globally, the combination-based bias correction methods (MMM, linear- and  $\alpha$ -pooling) show some robustness in their application to future projections, with uncertainties and sensitivities to the chosen models not being much different from those of the more usual CDF-t technique for precipitation, and being even smaller for temperature.

## 6 Conclusions and perspectives

495 In this study, we propose a new approach to perform bias correction of climate simulations, taking advantage of combinations  
of climate models. Combinations are realised via mathematical pooling of cumulative distribution functions (CDFs) – charac-  
terising the variable of interest as simulated by the climate models – to provide a new CDF designed to be more realistic, i.e.,  
closer to a reference CDF over the calibration period. It is important to emphasise that the proposed approach differs from the  
averaging of quantiles for a given probability as in Markiewicz et al. (2020). It also differs from the usual probability density  
500 aggregation, also sometimes called probability fusion (Koliander et al., 2022). Indeed, in our approach, we aggregate cumula-  
tive probability distributions. Moreover, our aggregation is indirect in that we aggregate transformed scores instead of directly  
aggregating the probabilities. In the later case, we would be restricted to weights summing to 1, whereas in our approach there  
is no such restriction.

Three pooling strategies have been tested: a CDF multi-model mean (MMM), a linear pooling and a new approach named  
505  $\alpha$ -pooling that allows more flexibility, as well as a more traditional bias correction method (CDF-t) applied separately model-  
by-model. These four methods have been compared with three different experiments relying on (i) an evaluation with respect to  
ERA5 reanalyses over a historical period, (ii) a perfect model experiment (PME) over future time periods and (iii) a sensitivity  
analysis to the choice of the climate models to combine.

In a cross-validation framework over the historical period (experiment (i), section 5.1), the four methods generally behave  
510 similarly, with most biases relatively well centered around 0, both in temperature and precipitation. However, the application  
of the “pure” bias correction method CDF-t on separate GCMs can generate more biases, with more variability. This is because  
the change (in temperature or precipitation) simulated by a single climate model over the historical period may not correspond  
to the change present in the reanalyses. By combining CDFs coming from different GCMs, the pooling techniques are also  
combining the evolution (i.e., changes) over time, resulting in bias corrected projections that are more consistent with the  
515 reanalyses.

The results of the PME experiment show a good robustness of the three pooling strategies, even for the MMM approach, with  
biases of most statistics (including extremes) around 0. Moreover, the biases in high quantiles, especially for maximum values,  
are much lower for pooling-based methods than for traditional BC methods represented here by CDF-t. Overall, a quasi-  
systematic ranking of the four methods is observed in this PME: while CDF-t can present some recurrent and pronounced  
520 biases – getting larger for further time periods –, the MMM correction approach improves the results, the linear approach even  
more and the best results are obtained with the  $\alpha$ -pooling-pooling technique for both variables. This confirms the interest of  
combining the information (here CDFs) from different models to perform bias correction, even in a strong climate change  
context. This is in agreement with results from Vrac et al. (2022) who showed, in a slightly different context, that accounting  
for the evolution of the mean temperature-precipitation correlation in an ensemble of climate models allows to get more robust  
525 estimates of future dependencies.

However, the CDFs resulting of our linear or  $\alpha$ -pooling approaches might depend on the selected ensemble of model CDFs to combine. Hence, the choice of the models to combine remains key as it necessarily influences the results over the (future) projection periods. Note, nevertheless, that this is true for any combination strategy – i.e., not only our proposed pooling methods – or for any bias correction technique where the choice of the model simulation to correct will also necessarily  
530 affect the final results (e.g., time series, CDFs, etc.). We also note here that for the combination methods that include weights (i.e. linear- and  $\alpha$ -pooling), the numerical optimization of the weights results in redundant CDFs to receive low weights. For instance, if two models result in the exact same CDF, the optimization will result in weights that will be shared between these identical CDFs and whose total would be the weight corresponding to this CDF not being duplicated. This is an important feature as it is known that some models are closely related and, thus, tend to provide similar forecasts.

535 The sensitivity analysis of the future (2081-2100) CDFs to the choice of the ensemble of models shows that the uncertainty in long-term projections was found globally comparable for the three pooling-based methods, although slightly higher for  $\alpha$ -pooling and slightly lower for MMM pooling. Indeed, as the  $\alpha$ - and linear-pooling associate non-uniform weights to the different CDFs, they pull the results towards the models with the highest weights, hence generating more variability depending on the selected ensemble of models to combine. Conversely, the MMM pooling corresponds to a linear pooling with weights  
540 forced to be uniform. Therefore, it provides smoother CDF results, less sensitive to the choice of the ensemble. The opposite example is given by CDF-t that is applied model-by-model and thus shows a high sensitivity to the selected ensemble. While MMM-pooling has the potential to lead to overly confident projections, our novel pooling method may offer a more realistic representation of scenario uncertainty. Nevertheless, it is crucial to acknowledge the potential for our  $\alpha$ -pooling method to introduce unrealistic scenario uncertainty. This aspect warrants further investigation in future studies, especially for practical  
545 applications.

In terms of computation time, it is obvious that alpha-pooling is more computationally demanding than linear- or MMM-pooling. This is in part due to the additional parameter  $\alpha$ , but mostly to the nonlinearity induced by  $\alpha$ -pooling. However, for the combination of up to 10 climate models (i.e., CDFs), the computational time for each location and variable time series typically does not exceed a few minutes. Given the substantial computational demands associated with running individual  
550 climate models, the computational aspect of combining them is trivial by comparison. Moreover, considering that this post-processing of climate simulations does not need to be performed on a daily basis but rather once for all, we believe that this represents a reasonable computational cost, ensuring the method's practical applicability without compromise.

As a conclusion, the  $\alpha$ -pooling model appears as a promising approach for pooling model CDFs. More generally, the results of this study show that the CDFs pooling strategy for “multi-model bias correction” is a credible alternative to usual GCM-by-  
555 GCM correction methods, by allowing to handle and consider several climate models at once.

This work can be extended in various ways. First, even though only temperature and precipitation were considered in this study, many other climate variables – such as wind, humidity, etc. – can be handled with this CDF-pooling strategy. Also, the

proposed pooling method can be directly applied to regional climate model simulations, instead of GCM simulations, in order to get more regional views about climate changes.

560 In addition, some more technical and statistical developments could be made to improve the CDF-pooling approach. For example, the present linear- and  $\alpha$ -pooling methods are based on the  $L2$  norm to estimate the parameters. Other distances could be used, and more specifically distances between distribution functions, e.g., the Hellinger distance, the total variation distance (Clarotto et al., 2022), the Wasserstein distance (e.g., Santambrogio, 2015; Robin et al., 2019) or the Kullback-Leibler divergence (Kullback and Leibler, 1951). Such distribution-based distances could potentially improve the quality of the fit and  
565 then provide more robust pooled CDFs.

Moreover, even though spatial patterns are visible in the parameters, there is a variability between nearby grid cells that complicates the interpretation of the parameters (see Fig. 3 and 4). Such a variability can be reduced by constraining the approach to provide more continuous and smoother spatial structures, presumably at the cost of longer computations.

Note also that it would be interesting to account for rainfall specificities when applying a CDF-pooling strategy to precipitation.  
570 Indeed, in this study, the pooling was applied to all daily precipitation values. In practice, a distinction between dry days frequencies and distributions of wet intensity could be made by having two separate poolings. Although the  $\alpha$ -pooling results for precipitation in this article were quite satisfying, such a rainfall-specific design could provide additional improvements and would deserve to be tested in the future.

Other modelling extensions could be considered. One interesting aspect could be to focus on extreme events. For example,  
575  $\alpha$ -pooling could be applied to conditional CDFs above a high threshold related to the tail of the whole distribution, or applied to the CDF of block-maxima. Distributions stemming from the extreme values theory – such as the Generalized Pareto Distribution (GPD) or the Generalized Extreme Value distribution (GEV) – would then have to be used. Behind the practical results that such an application could bring, the statistical properties of the resulting pooled (extreme) CDFs would also be worth studying from the theoretical point-of-view.

580 Another interesting perspective, both from the practical and theoretical aspects, concerns the extension of the  $\alpha$ -pooling to the multivariate context. Indeed, so far, this pooling method has been developed and applied only in a univariate framework, i.e., different variables (temperature and precipitation) are handled, combined and bias corrected separately. An extension of  $\alpha$ -pooling allowing to combine joint (i.e., multivariate) CDFs would allow improving the modelling of dependencies between the variables and, thus, to provide more realistic inter-variable CDFs and bias corrected projections. Such an extended  $\alpha$ -pooling  
585 should then be compared to other multivariate bias correction methods, such as those studied in François et al. (2020) for example. It would then also allow investigating compound events (e.g., Zscheischler et al., 2018, 2020) and their potential future changes more robustly.

Finally, more generally, it is worth noticing that combination and bias correction are not new questions or requirements. However, this is the first paper coupling methods from these two domains. This was made possible by our pooling strategy  
590 working on CDFs (and not on specific quantiles or statistical properties such as mean, max, etc., as usually done), which

is, in itself, an original contribution to the combination framework. This CDF-pooling strategy and this hybrid combination-correction method deserve to be further explored, as well as its potential applications beyond combination and bias correction.

## **Acknowledgments**

We acknowledge the World Climate Research Programme’s Working Group on Coupled Modelling, which is responsible for  
595 CMIP, and we thank the climate modeling groups (listed in Table 1 of this paper) for producing and making available their models outputs. For CMIP, the U.S. Department of Energy’s Program for Climate Model Diagnosis and Intercomparison provides coordinating support and led development of software infrastructure in partnership with the Global Organization for Earth System Science Portals. We also thank the Copernicus Climate Change Services for making the ERA5 reanalyses available.

600 This work has been supported by the “COMBINE” project funded by the Swiss National Science Foundation grant n° 200021\_200337 / 1, as well as by the “COESION” project funded by the French National program LEFE (Les Enveloppes Fluides et l’Environnement). MV’s work also benefited from state aid managed by the National Research Agency under France 2030 bearing the references ANR-22-EXTR-0005 (TRACCS-PC4-EXTENDING project) and ANR-22EXTR-0011 (TRACCS-PC10-LOCALISING project). The authors also acknowledge the support of the INRAE / Mines Paris chair “Geolearning”.

## **605 Authors’ contributions**

MV and GM had the initial idea of the study, which has been completed and enriched by all co-authors. DA developed the initial mathematical framework and derived the main theoretical properties, helped by MV, ST and GM. MV and DA developed the codes for inferring the  $\alpha$ -pooling parameters. MV applied it to CMIP6 simulations for the different experiments and wrote the codes for the analyses and to plot the figures. All authors contributed to the methodology and the analyses. MV wrote the  
610 first draft of the article with inputs from all the co-authors.

## **Competing interests**

The authors declare that no competing interests are present.

## **Data availability**

The CMIP6 model simulations can be downloaded through the Earth System Grid Federation portals. Instructions to access the  
615 data are available here: <https://pcmdi.llnl.gov/mips/cmip6/data-access-getting-started.html>. The ERA5 reanalysis data used as reference in this study can be accessed via the “Climate Data Store” (CDS) web portal <https://cds.climate.copernicus.eu>.

## References

- Abramowitz, G., Herger, N., Gutmann, E., Hammerling, D., Knutti, R., Leduc, M., Lorenz, R., Pincus, R., and Schmidt, G. A.: ESD Reviews: Model dependence in multi-model climate ensembles: weighting, sub-selection and out-of-sample testing, 10, 91–105, <https://doi.org/10.5194/esd-10-91-2019>, publisher: Copernicus GmbH, 2019.
- 620 Ahmed, K., Sachindra, D. A., Shahid, S., Demirel, M. C., and Chung, E.-S.: Selection of multi-model ensemble of general circulation models for the simulation of precipitation and maximum and minimum temperature based on spatial assessment metrics, 23, 4803–4824, <https://doi.org/10.5194/hess-23-4803-2019>, publisher: Copernicus GmbH, 2019.
- Allard, D., Comunian, A., and Renard, P.: Probability aggregation methods in geoscience, *Mathematical Geosciences*, 44, 545–581, 2012.
- 625 Arias, P., Bellouin, N., Coppola, E., Jones, R., Krinner, G., Marotzke, J., Naik, V., Palmer, M., Plattner, G.-K., Rogelj, J., Rojas, M., Sillmann, J., Storelvmo, T., Thorne, P., Trewin, B., Achuta Rao, K., Adhikary, B., Allan, R., Armour, K., Bala, G., Barimalala, R., Berger, S., Canadell, J., Cassou, C., Cherchi, A., Collins, W., Collins, W., Connors, S., Corti, S., Cruz, F., Dentener, F., Dereczynski, C., Di Luca, A., Diongue Niang, A., Doblas-Reyes, F., Dosio, A., Douville, H., Engelbrecht, F., Eyring, V., Fischer, E., Forster, P., Fox-Kemper, B., Fuglestedt, J., Fyfe, J., Gillett, N., Goldfarb, L., Gorodetskaya, I., Gutierrez, J., Hamdi, R., Hawkins, E., Hewitt, H., Hope, P., Islam, A., Jones, C., Kaufman, D., Kopp, R., Kosaka, Y., Kossin, J., Krakovska, S., Lee, J.-Y., Li, J., Mauritsen, T., Maycock, T., Meinshausen, M., Min, S.-K., Monteiro, P., Ngo-Duc, T., Otto, F., Pinto, I., Pirani, A., Raghavan, K., Ranasinghe, R., Ruane, A., Ruiz, L., Sallée, J.-B., Samset, B., Sathyendranath, S., Seneviratne, S., Sörensson, A., Szopa, S., Takayabu, I., Tréguier, A.-M., van den Hurk, B., Vautard, R., von Schuckmann, K., Zaehle, S., Zhang, X., and Zickfeld, K.: Technical Summary, in: *Climate Change 2021: The Physical Science Basis. Contribution of Working Group I to the Sixth Assessment Report of the Intergovernmental Panel on Climate Change*, edited by Masson-Delmotte, V., Zhai, P., Pirani, A., Connors, S., Péan, C., Berger, S., Caud, N., Chen, Y., Goldfarb, L., Gomis, M., Huang, M., Leitzell, K., Lonnoy, E., Matthews, J., Maycock, T., Waterfield, T., Yelekçi, O., Yu, R., and Zhou, B., pp. 33–144, Cambridge University Press, <https://doi.org/10.1017/9781009157896.002>, 2021.
- 630 Bhat, K. S., Haran, M., Terando, A., and Keller, K.: Climate Projections Using Bayesian Model Averaging and Space–Time Dependence, 16, 606–628, <https://doi.org/10.1007/s13253-011-0069-3>, 2011.
- 640 Bordley, R.: A multiplicative formula for aggregating probability assessments, *Management Science*, 28, 1137–1148, 1982.
- Boucher, O., Denvil, S., Levassasseur, G., Cozic, A., Caubel, A., Foujols, M.-A., Meurdesoif, Y., Cadule, P., Devilliers, M., Ghattas, J., Lebas, N., Lurton, T., Mellul, L., Musat, I., Mignot, J., and Cheruy, F.: IPSL IPSL-CM6A-LR model output prepared for CMIP6 CMIP, <https://doi.org/10.22033/ESGF/CMIP6.1534>, 2018.
- Brier, G. W. et al.: Verification of forecasts expressed in terms of probability, *Monthly weather review*, 78, 1–3, 1950.
- 645 Brunner, L., McSweeney, C., Ballinger, A. P., Befort, D. J., Benassi, M., Booth, B., Coppola, E., de Vries, H., Harris, G., Hegerl, G. C., Knutti, R., Lenderink, G., Lowe, J., Nogherotto, R., O’Reilly, C., Qasmi, S., Ribes, A., Stocchi, P., and Undorf, S.: Comparing Methods to Constrain Future European Climate Projections Using a Consistent Framework, *Journal of Climate*, 33, 8671 – 8692, <https://doi.org/https://doi.org/10.1175/JCLI-D-19-0953.1>, 2020.
- Bukovsky, M., Thompson, J., and L.O., M.: Weighting a regional climate model ensemble: Does it make a difference? Can it make a difference?, 77, 23–43, <https://doi.org/10.3354/cr01541>, 2019.
- 650 Byrd, R. H., Lu, P., Nocedal, J., and Zhu, C.: A Limited Memory Algorithm for Bound Constrained Optimization, *SIAM Journal on Scientific Computing*, 16, 1190–1208, <https://doi.org/10.1137/0916069>, 1995.
- Cannon, A. J., Sobie, S. R., and Murdock, T. Q.: Bias Correction of GCM Precipitation by Quantile Mapping: How Well Do Methods Preserve Changes in Quantiles and Extremes?, *Journal of Climate*, 28, 6938–6959, <https://doi.org/10.1175/JCLI-D-14-00754.1>, 2015.

- 655 Clarotto, L., Allard, D., and Menafoglio, A.: A new class of  $\alpha$ -transformations for the spatial analysis of Compositional Data, *Spatial Statistics*, 47, 100–570, <https://doi.org/https://doi.org/10.1016/j.spasta.2021.100570>, 2022.
- Danabasoglu, G., Lamarque, J.-F., Bacmeister, J., Bailey, D. A., DuVivier, A. K., Edwards, J., Emmons, L. K., Fasullo, J., Garcia, R., Gettelman, A., Hannay, C., Holland, M. M., Large, W. G., Lauritzen, P. H., Lawrence, D. M., Lenaerts, J. T. M., Lindsay, K., Lipscomb, W. H., Mills, M. J., Neale, R., Oleson, K. W., Otto-Bliesner, B., Phillips, A. S., Sacks, W., Tilmes, S., van Kampenhout, L., Vertenstein, M., Bertini, A., Dennis, J., Deser, C., Fischer, C., Fox-Kemper, B., Kay, J. E., Kinnison, D., Kushner, P. J., Larson, V. E., Long, M. C., Mickelson, S., Moore, J. K., Nienhouse, E., Polvani, L., Rasch, P. J., and Strand, W. G.: The Community Earth System Model Version 2 (CESM2), *Journal of Advances in Modeling Earth Systems*, 12, e2019MS001916, <https://doi.org/https://doi.org/10.1029/2019MS001916>, 2020.
- 660 de Elía, R., Laprise, R., and Denis, B.: Forecasting Skill Limits of Nested, Limited-Area Models: A Perfect-Model Approach, *Monthly Weather Review*, 130, 2006–2023, [https://doi.org/10.1175/1520-0493\(2002\)130<2006:FSLONL>2.0.CO;2](https://doi.org/10.1175/1520-0493(2002)130<2006:FSLONL>2.0.CO;2), 2002.
- Dembélé, M., Ceperley, N., Zwart, S. J., Salvadore, E., Mariethoz, G., and Schaeffli, B.: Potential of satellite and re-analysis evaporation datasets for hydrological modelling under various model calibration strategies, 143, 103–667, <https://doi.org/10.1016/j.advwatres.2020.103667>, 2020.
- Déqué, M.: Frequency of precipitation and temperature extremes over France in an anthropogenic scenario: Model results and statistical 670 correction according to observed values, *Global Planet. Change*, 57, 16–26, 2007.
- Eden, J., Widmann, M., Grawe, D., and Rast, S.: Skill, Correction, and Downscaling of GCM-Simulated Precipitation, *J. Climate*, 25, 3970–3984, <https://doi.org/https://doi.org/10.1175/JCLI-D-11-00254.1>, 2012.
- Eyring, V., Bony, S., Meehl, G. A., Senior, C. A., Stevens, B., Stouffer, R. J., and Taylor, K. E.: Overview of the Coupled Model Intercomparison Project Phase 6 (CMIP6) experimental design and organization, *Geoscientific Model Development*, 9, 1937–1958, 675 <https://doi.org/10.5194/gmd-9-1937-2016>, 2016.
- Fragoso, T. M., Bertoli, W., and Louzada, F.: Bayesian model averaging: A systematic review and conceptual classification, *International Statistical Review*, 86, 1–28, 2018.
- François, B., Vrac, M., Cannon, A. J., Robin, Y., and Allard, D.: Multivariate bias corrections of climate simulations: which benefits for which losses?, *Earth System Dynamics*, 11, 537–562, <https://doi.org/10.5194/esd-11-537-2020>, 2020.
- 680 François, B., Thao, S., and Vrac, M.: Adjusting spatial dependence of climate model outputs with Cycle-Consistent Adversarial Networks, *Clim Dyn*, p. 3323–3353, <https://doi.org/10.1007/s00382-021-05869-8>, 2021.
- Gneiting, T. and Katzfuss, M.: Probabilistic Forecasting, 1, 125–151, <https://doi.org/10.1146/annurev-statistics-062713-085831>, [\\_eprint: https://doi.org/10.1146/annurev-statistics-062713-085831](https://doi.org/10.1146/annurev-statistics-062713-085831), 2014.
- Gneiting, T. and Raftery, A. E.: Strictly proper scoring rules, prediction, and estimation, *Journal of the American statistical Association*, 102, 685 359–378, 2007.
- Gudmundsson, L., Bremnes, J. B., Haugen, J. E., and Engen-Skaugen, T.: Technical Note: Downscaling RCM precipitation to the station scale using statistical transformations – a comparison of methods, *Hydrology and Earth System Sciences*, 16, 3383–3390, <https://doi.org/10.5194/hess-16-3383-2012>, 2012.
- Haddad, Z. and Rosenfeld, D.: Optimality of empirical z-r relations, *Q. J. R. Meteorol. Soc.*, 123, 1283–1293, 1997.
- 690 Held, I. M., Guo, H., Adcroft, A., Dunne, J. P., Horowitz, L. W., Krasting, J., Shevliakova, E., Winton, M., Zhao, M., Bushuk, M., Wittenberg, A. T., Wyman, B., Xiang, B., Zhang, R., Anderson, W., Balaji, V., Donner, L., Dunne, K., Durachta, J., Gauthier, P. P. G., Ginoux, P., Golaz, J.-C., Griffies, S. M., Hallberg, R., Harris, L., Harrison, M., Hurlin, W., John, J., Lin, P., Lin, S.-J., Malyshev, S., Menzel, R., Milly, P. C. D.,

- Ming, Y., Naik, V., Paynter, D., Paulot, F., Ramaswamy, V., Reichl, B., Robinson, T., Rosati, A., Seman, C., Silvers, L. G., Underwood, S., and Zadeh, N.: Structure and Performance of GFDL's CM4.0 Climate Model, *Journal of Advances in Modeling Earth Systems*, 11, 3691–3727, <https://doi.org/https://doi.org/10.1029/2019MS001829>, 2019.
- 695
- Hersbach, H., Bell, B., Berrisford, P., Hirahara, S., Horányi, A., Muñoz-Sabater, J., Nicolas, J., Peubey, C., Radu, R., Schepers, D., Simmons, A., Soci, C., Abdalla, S., Abellan, X., Balsamo, G., Bechtold, P., Biavati, G., Bidlot, J., Bonavita, M., De Chiara, G., Dahlgren, P., Dee, D., Diamantakis, M., Dragani, R., Flemming, J., Forbes, R., Fuentes, M., Geer, A., Haimberger, L., Healy, S., Hogan, R. J., Hólm, E., Janisková, M., Keeley, S., Laloyaux, P., Lopez, P., Lupu, C., Radnoti, G., de Rosnay, P., Rozum, I., Vamborg, F., Vil-  
700 laume, S., and Thépaut, J.-N.: The ERA5 global reanalysis, *Quarterly Journal of the Royal Meteorological Society*, 146, 1999–2049, <https://doi.org/https://doi.org/10.1002/qj.3803>, 2020.
- Intergovernmental Panel on Climate Change (IPCC): Evaluation of Climate Models, in: *Climate Change 2013 – The Physical Science Basis: Working Group I Contribution to the Fifth Assessment Report of the Intergovernmental Panel on Climate Change*, edited by Intergovernmental Panel on Climate Change (IPCC), pp. 741–866, Cambridge University Press, <https://doi.org/10.1017/CBO9781107415324.020>,  
705 2014.
- IPCC: *Climate Change 2021 – The Physical Science Basis: Working Group I Contribution to the Sixth Assessment Report of the Intergovernmental Panel on Climate Change*, Cambridge University Press, 1 edn., <https://doi.org/10.1017/9781009157896>, 2023.
- Kleiber, W., Raftery, A. E., and Gneiting, T.: Geostatistical Model Averaging for Locally Calibrated Probabilistic Quantitative Precipitation Forecasting, 106, 1291–1303, <https://doi.org/10.1198/jasa.2011.ap10433>, publisher: Taylor & Francis \_eprint:  
710 <https://doi.org/10.1198/jasa.2011.ap10433>, 2011.
- Knutti, R., Sedláček, J., Sanderson, B. M., Lorenz, R., Fischer, E. M., and Eyring, V.: A climate model projection weighting scheme accounting for performance and interdependence: Model Projection Weighting Scheme, <https://doi.org/10.1002/2016GL072012>, 2017.
- Koliander, G., El-Laham, Y., Djurić, P. M., and Hlawatsch, F.: Fusion of probability density functions, *Proceedings of the IEEE*, 110, 404–453, 2022.
- 715 Krinner, G. and Flanner, M. G.: Striking stationarity of large-scale climate model bias patterns under strong climate change, *Proceedings of the National Academy of Sciences*, 115, 9462–9466, <https://doi.org/10.1073/pnas.1807912115>, 2018.
- Kullback, S. and Leibler, R. A.: On information and sufficiency, *The annals of mathematical statistics*, 22, 79–86, 1951.
- Kwatra, V., Schödl, A., Essa, I., Turk, G., and Bobick, A.: Graphcut Textures: Image and Video Synthesis Using Graph Cuts, *ACM Trans. Graph.*, 22, 277–286, <https://doi.org/10.1145/882262.882264>, 2003.
- 720 Lange, S.: ISIMIP3b bias adjustment fact sheet, Technical report, ISIMIP, [https://www.isimip.org/documents/413/ISIMIP3b\\_bias\\_adjustment\\_fact\\_sheet\\_Gnsz7CO.pdf](https://www.isimip.org/documents/413/ISIMIP3b_bias_adjustment_fact_sheet_Gnsz7CO.pdf), 2021.
- Lange, S. and Büchner, M.: ISIMIP3b bias-adjusted atmospheric climate input data, <https://doi.org/10.48364/ISIMIP.842396.1>, 2021.
- Markiewicz, I., Bogdanowicz, E., and Kochanek, K.: Quantile Mixture and Probability Mixture Models in a Multi-Model Approach to Flood Frequency Analysis, *Water*, 12, <https://doi.org/10.3390/w12102851>, 2020.
- 725 Michelangeli, P., Vrac, M., and Loukos, H.: Probabilistic downscaling approaches: application to wind cumulative distribution functions, *Geophys. Res. Lett.*, 36, L11 708, doi:10.1029/2009GL038 401, 2009.
- Neyman, E. and Roughgarden, T.: From Proper Scoring Rules to Max-Min Optimal Forecast Aggregation, *Operations Research*, 2023.
- Olson, R., Fan, Y., and Evans, J. P.: A simple method for Bayesian model averaging of regional climate model projections: Application to southeast Australian temperatures, 43, 7661–7669, <https://doi.org/10.1002/2016GL069704>, \_eprint:  
730 <https://onlinelibrary.wiley.com/doi/pdf/10.1002/2016GL069704>, 2016.



- Panofsky, H. and Brier, G.: Some applications of statistics to meteorology, Earth and Mineral Sciences Continuing Education, College of Earth and Mineral Sciences, 103 pp., 1968.
- Ribes, A., Zwiers, F. W., Azaïs, J.-M., and Naveau, P.: A new statistical approach to climate change detection and attribution, *Climate Dynamics*, 48, 367–386, 2017.
- 735 Robin, Y. and Vrac, M.: Is time a variable like the others in multivariate statistical downscaling and bias correction?, *Earth System Dynamics Discussions*, 2021, 1–32, <https://doi.org/10.5194/esd-2021-12>, 2021.
- Robin, Y., Vrac, M., Naveau, P., and Yiou, P.: Multivariate stochastic bias corrections with optimal transport, *Hydrol. Earth Syst. Sci.*, 23, 773–786, <https://doi.org/10.5194/hess-23-773-2019>, 2019.
- Rougier, J., Goldstein, M., and House, L.: Second-Order Exchangeability Analysis for Multimodel Ensembles, 108, 852–863, <https://doi.org/10.1080/01621459.2013.802963>, publisher: Taylor & Francis \_eprint: <https://doi.org/10.1080/01621459.2013.802963>, 2013.
- 740 Sain, S. and Cressie, N.: A spatial model for multivariate lattice data, pp. 226–259, <https://doi.org/10.1016/j.jeconom.2006.09.010>, 2007.
- Sanderson, B. M., Wehner, M., and Knutti, R.: Skill and independence weighting for multi-model assessments, *Geoscientific Model Development*, 10, 2379–2395, <https://doi.org/10.5194/gmd-10-2379-2017>, 2017.
- 745 Santambrogio, F.: Optimal Transport for Applied Mathematicians: Calculus of Variations, PDEs, and Modeling, *Progress in Nonlinear Differential Equations and Their Applications*, Birkhäuser, Cham, 1 edn., <https://doi.org/https://doi.org/10.1007/978-3-319-20828-2>, 2015.
- Schmidli, J., Frei, C., and Vidale, P.: Downscaling from GCM precipitation: a benchmark for dynamical and statistical downscaling methods, *International Journal of Climatology*, 26, 679–689, <https://doi.org/10.1002/joc.1287>, 2006.
- Shiogama, H., Abe, M., and Tatebe, H.: MIROC MIROC6 model output prepared for CMIP6 ScenarioMIP, <https://doi.org/10.22033/ESGF/CMIP6.898>, 2019.
- 750 Stott, P.: How climate change affects extreme weather events, 352, 1517–1518, <https://doi.org/10.1126/science.aaf7271>, publisher: American Association for the Advancement of Science, 2016.
- Strobach, E. and Bel, G.: Learning algorithms allow for improved reliability and accuracy of global mean surface temperature projections, 11, 451, <https://doi.org/10.1038/s41467-020-14342-9>, number: 1 Publisher: Nature Publishing Group, 2020.
- 755 Swart, N. C., Cole, J. N., Kharin, V. V., Lazare, M., Scinocca, J. F., Gillett, N. P., Anstey, J., Arora, V., Christian, J. R., Jiao, Y., Lee, W. G., Majaess, F., Saenko, O. A., Seiler, C., Seinen, C., Shao, A., Solheim, L., von Salzen, K., Yang, D., Winter, B., and Sigmund, M.: CCCma CanESM5 model output prepared for CMIP6 ScenarioMIP, <https://doi.org/10.22033/ESGF/CMIP6.1317>, 2019.
- Tang, Y., Rumbold, S., Ellis, R., Kelley, D., Mulcahy, J., Sellar, A., Walton, J., and Jones, C.: MOHC UKESM1.0-LL model output prepared for CMIP6 CMIP historical, <https://doi.org/10.22033/ESGF/CMIP6.6113>, 2019.
- 760 Thao, S., Garvik, M., Mariétoz, G., and M.Vrac: Combining Global Climate Models Using Graph Cuts, *Clim. Dyn.*, 59, 2345–2361, <https://doi.org/10.1007/s00382-022-06213-4>, 2022.
- Thorarinsdottir, T. L. and Gneiting, T.: Probabilistic forecasts of wind speed: ensemble model output statistics by using heteroscedastic censored regression, 173, 371–388, <https://doi.org/10.1111/j.1467-985X.2009.00616.x>, \_eprint: <https://onlinelibrary.wiley.com/doi/pdf/10.1111/j.1467-985X.2009.00616.x>, 2010.
- 765 Voldoire, A.: CNRM-CERFACS CNRM-CM6-1-HR model output prepared for CMIP6 HighResMIP, <https://doi.org/10.22033/ESGF/CMIP6.1387>, 2019.

- Volodin, E., Mortikov, E., Gritsun, A., Lykossov, V., Galin, V., Diansky, N., Gusev, A., Kostykin, S., Iakovlev, N., Shestakova, A., and Emelina, S.: INM INM-CM5-0 model output prepared for CMIP6 CMIP abrupt-4xCO2, <https://doi.org/10.22033/ESGF/CMIP6.4932>, 2019.
- 770 Vrac, M.: Multivariate bias adjustment of high-dimensional climate simulations: the Rank Resampling for Distributions and Dependences (R2D2) bias correction, *Hydrology and Earth System Sciences*, 22, 3175–3196, <https://doi.org/https://doi.org/10.5194/hess-22-3175-2018>, 2018.
- Vrac, M. and Thao, S.: R<sup>2</sup>D<sup>2</sup> v2.0: accounting for temporal dependences in multivariate bias correction via analogue rank resampling, *Geoscientific Model Development*, 13, 5367–5387, <https://doi.org/10.5194/gmd-13-5367-2020>, 2020.
- 775 Vrac, M., Stein, M. L., Hayhoe, K., and Liang, X.-Z.: A general method for validating statistical downscaling methods under future climate change, *Geophysical Research Letters*, 34, <https://doi.org/https://doi.org/10.1029/2007GL030295>, 2007.
- Vrac, M., Drobinski, P., Merlo, A., Herrmann, M., Lavaysse, C., Li, L., and Somot, S.: Dynamical and statistical downscaling of the French Mediterranean climate: uncertainty assessment, *Nat. Hazards Earth Syst. Sci.*, 12, 2769–2784, doi:10.5194/nhess-12-2769-2012, 2012.
- Vrac, M., Noël, T., and Vautard, R.: Bias correction of precipitation through Singularity Stochastic Removal: Because occurrences matter, *Journal of Geophysical Research: Atmospheres*, 121, <https://doi.org/10.1002/2015JD024511>, 2016.
- 780 Vrac, M., Thao, S., and Yiou, P.: Should Multivariate Bias Corrections of Climate Simulations Account for Changes of Rank Correlation Over Time?, *Journal of Geophysical Research: Atmospheres*, 127, e2022JD036562, <https://doi.org/https://doi.org/10.1029/2022JD036562>, e2022JD036562 2022JD036562, 2022.
- Wanders, N. and Wood, E. F.: Improved sub-seasonal meteorological forecast skill using weighted multi-model ensemble simulations, 11, 094 007, <https://doi.org/10.1088/1748-9326/11/9/094007>, publisher: IOP Publishing, 2016.
- 785 Weigel, A. P., Knutti, R., Liniger, M. A., and Appenzeller, C.: Risks of Model Weighting in Multimodel Climate Projections, 23, 4175–4191, <https://doi.org/10.1175/2010JCLI3594.1>, publisher: American Meteorological Society Section: Journal of Climate, 2010.
- WGI, I.: Climate Change 2021: The Physical Science Basis. Contribution of Working Group I to the Sixth Assessment Report of the Intergovernmental Panel on Climate Change, Masson-Delmotte, V., P. Zhai, A. Pirani, S.L. Connors, C. Péan, S. Berger, N. Caud, Y. Chen, L. Goldfarb, M.I. Gomis, M. Huang, K. Leitzell, E. Lonnoy, J.B.R. Matthews, T.K. Maycock, T. Waterfield, O. Yelekçi, R. Yu, and B. Zhou (eds.), Cambridge University Press, 2021.
- 790 Wu, T., Chu, M., Dong, M., Fang, Y., Jie, W., Li, J., Li, W., Liu, Q., Shi, X., Xin, X., Yan, J., Zhang, F., Zhang, J., Zhang, L., and Zhang, Y.: BCC BCC-CSM2MR model output prepared for CMIP6 CMIP piControl, <https://doi.org/10.22033/ESGF/CMIP6.3016>, 2018.
- Wuebbles, D., Easterling, D., Hayhoe, K., Knutson, T., Kopp, R., Kossin, J., Kunkel, K., LeGrande, A., Mears, C., Sweet, W., Taylor, P., 795 Vose, R., Wehner, M., Wuebbles, D., Fahey, D., Hibbard, K., Dokken, D., Stewart, B., and Maycock, T.: Ch. 1: Our Globally Changing Climate. Climate Science Special Report: Fourth National Climate Assessment, Volume I, <https://doi.org/10.7930/J08S4N35>, 2017.
- Xu, C.-Y.: From GCMs to river flow: a review of downscaling methods and hydrologic modelling approaches, *Progress in Physical Geography*, 23, 229–249, <https://doi.org/10.1177/030913339902300204>, 1999.
- Yukimoto, S., Koshiro, T., Kawai, H., Oshima, N., Yoshida, K., Urakawa, S., Tsujino, H., Deushi, M., Tanaka, T., Hosaka, M., Yoshimura, 800 H., Shindo, E., Mizuta, R., Ishii, M., Obata, A., and Adachi, Y.: MRI MRI-ESM2.0 model output prepared for CMIP6 CMIP, <https://doi.org/10.22033/ESGF/CMIP6.621>, 2019.
- Zscheischler, J., Westra, S., van den Hurk, B., Seneviratne, S., Ward, P., Pitman, A., AghaKouchak, A., Bresch, D., Leonard, M., Wahl, T., and Zhang, X.: Future climate risk from compound events, *Nature Clim Change*, 8, 469–477, <https://doi.org/https://doi.org/10.1038/s41558-018-0156-3>, 2018.

805 Zscheischler, J., Martius, O., Westra, S., Bevacqua, E., Raymond, C., Horton, R., van den Hurk, B., AghaKouchak, A., Jézéquel, A., Mahecha, M., Maraun, D., Ramos, A., Ridder, N., Thiery, W., and Vignotto, E.: A typology of compound weather and climate events, *Nat Rev Earth Environ*, 1, 333—347, <https://doi.org/10.1038/s43017-020-0060-z>, 2020.

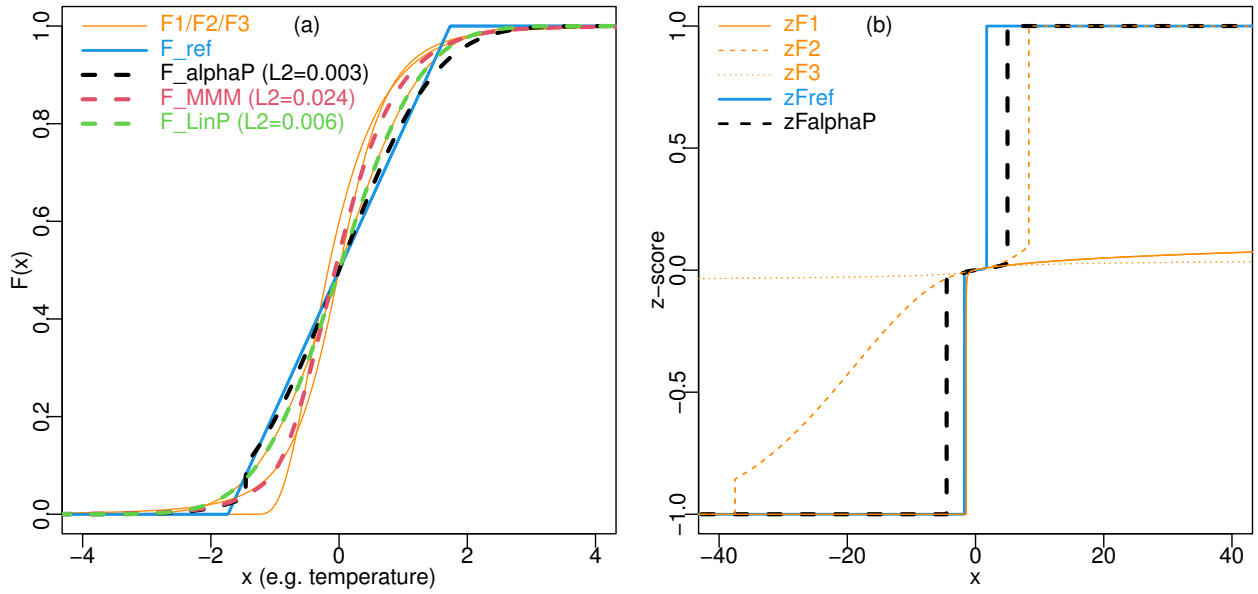


**Figure 1.** Illustration for  $N = 3$  distributions  $F_1, F_2$  and  $F_3$  to be combined, corresponding respectively to a log-normal CDF, a Gaussian one and a Student-t distribution. A Uniform CDF is arbitrarily fixed as reference. Note that the four CDFs are constructed here with same mean and variance to respect the constraints of our real-case application. Panel (a) displays the 3 CDFs to combine (orange lines), the reference CDF (blue line), as well as the resulting  $\alpha$ -pooling CDF (black dashed line), MMM CDF (red dashed line) and linear-pooling CDF (green dashed line). For each pooling method, the value of the  $L^2$  norm between the result CDF and the reference one (i.e., the quadratic distance  $Q$  in Eq. (10)) is also indicated. Note that the reference is not used to perform MMM. Panel (b) shows the z-scores (i.e., function  $G$  in Eq. (8) where  $z = G(F(x))$  with  $F(x)$  the CDF) for the 3 CDFs to be combined, the reference one and the  $\alpha$ -pooling CDF.

810

815

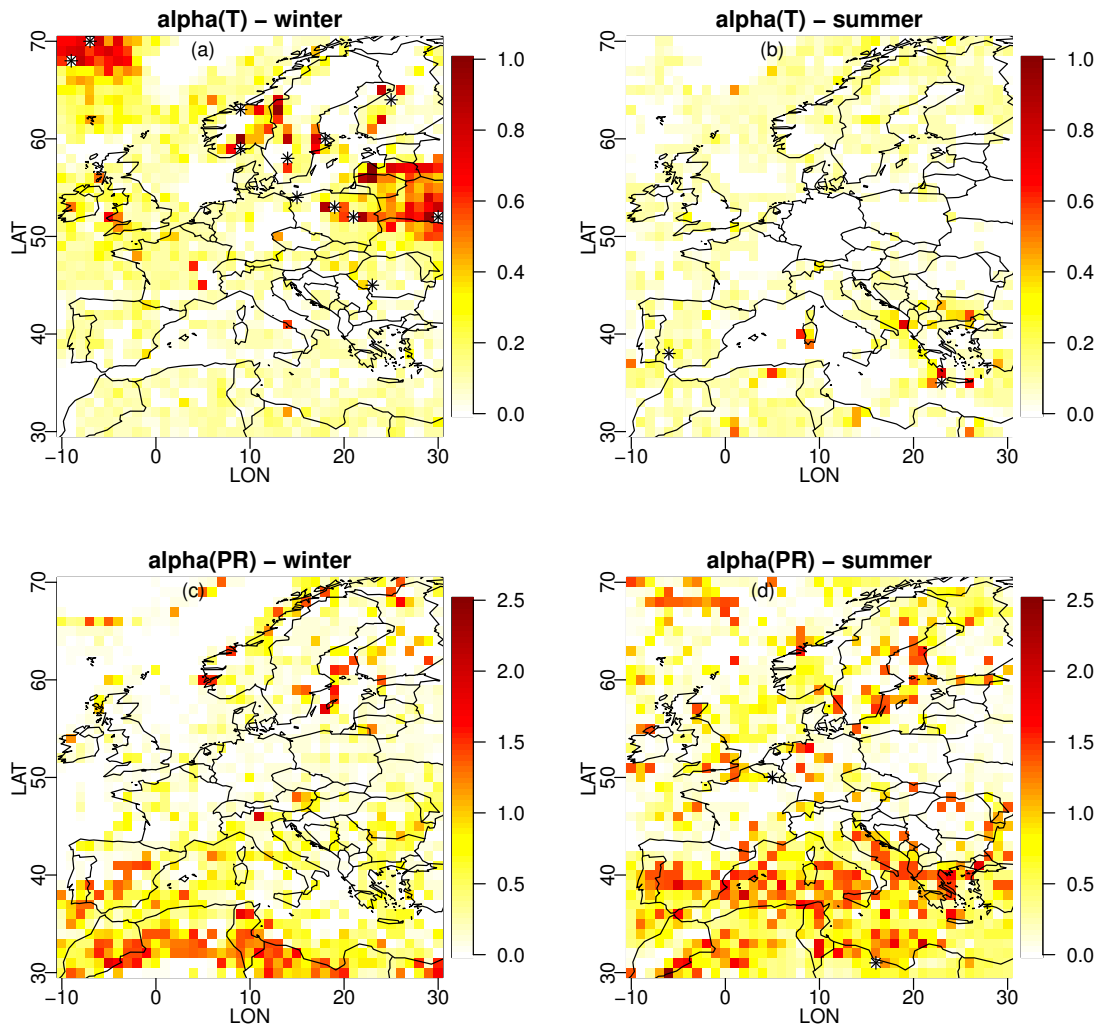


**Figure 2.** From  $\alpha$ -pooling, maps of the parameters  $\alpha$  obtained within the ERA5 experiment for temperature (a, b) and precipitation (c, d), over winter (a, c) and summer (b, d) seasons.

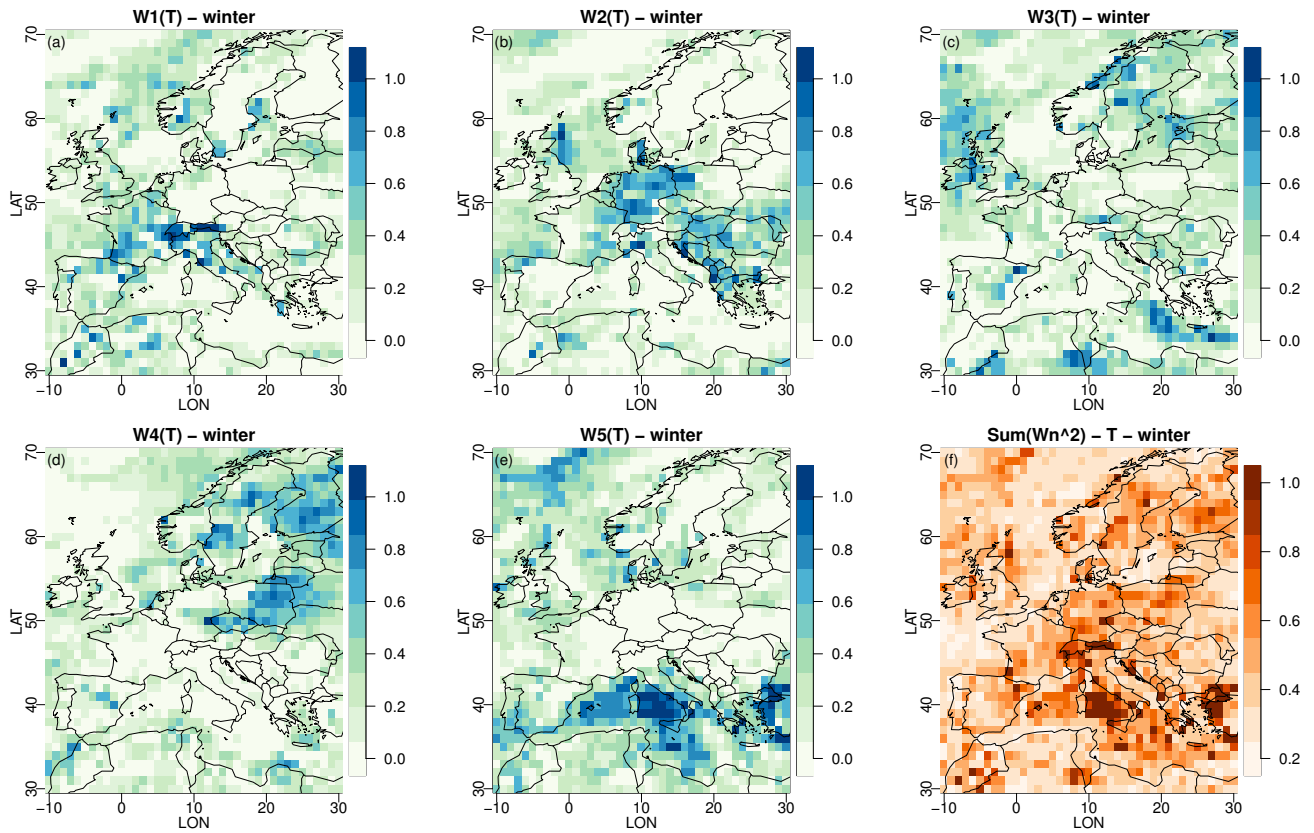


**Figure 3.** Maps of the weights parameters from  $\alpha$ -pooling for winter obtained with the ERA5 experiment for temperature, over winter. Models 1 to 5 correspond respectively to CNRM-CM6-1-HR, GFDL-CM4, IPSL-CM6A-LR, MRI-ESM2-0 and UKESM1-0-LL. Panel (f) displays the concentration index, equal to sum of the squares of the 5 normalized weights. The results for summer are given as supplementary information in Figure S1.

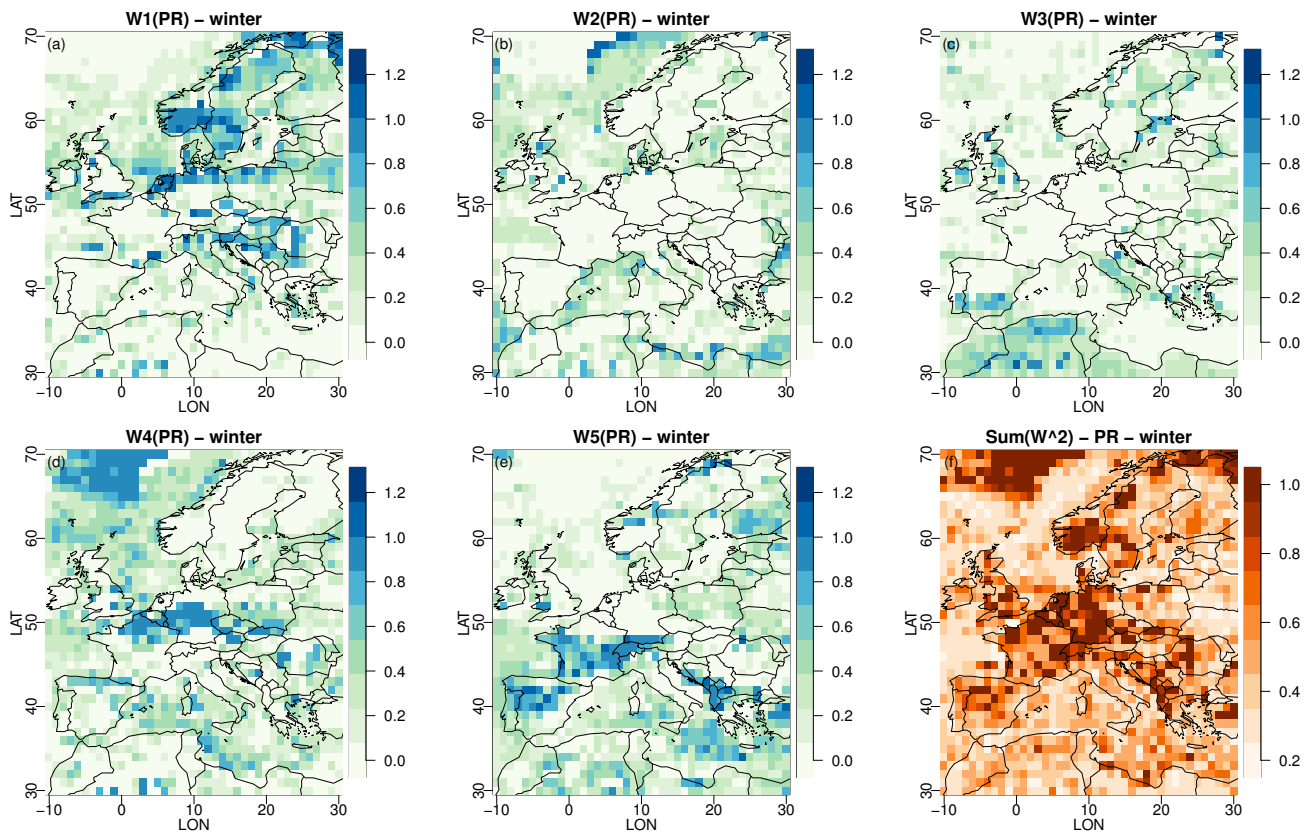


**Figure 4.** Same as Fig. 3 but for precipitation. The results for summer are given as supplementary information in Figure S2.

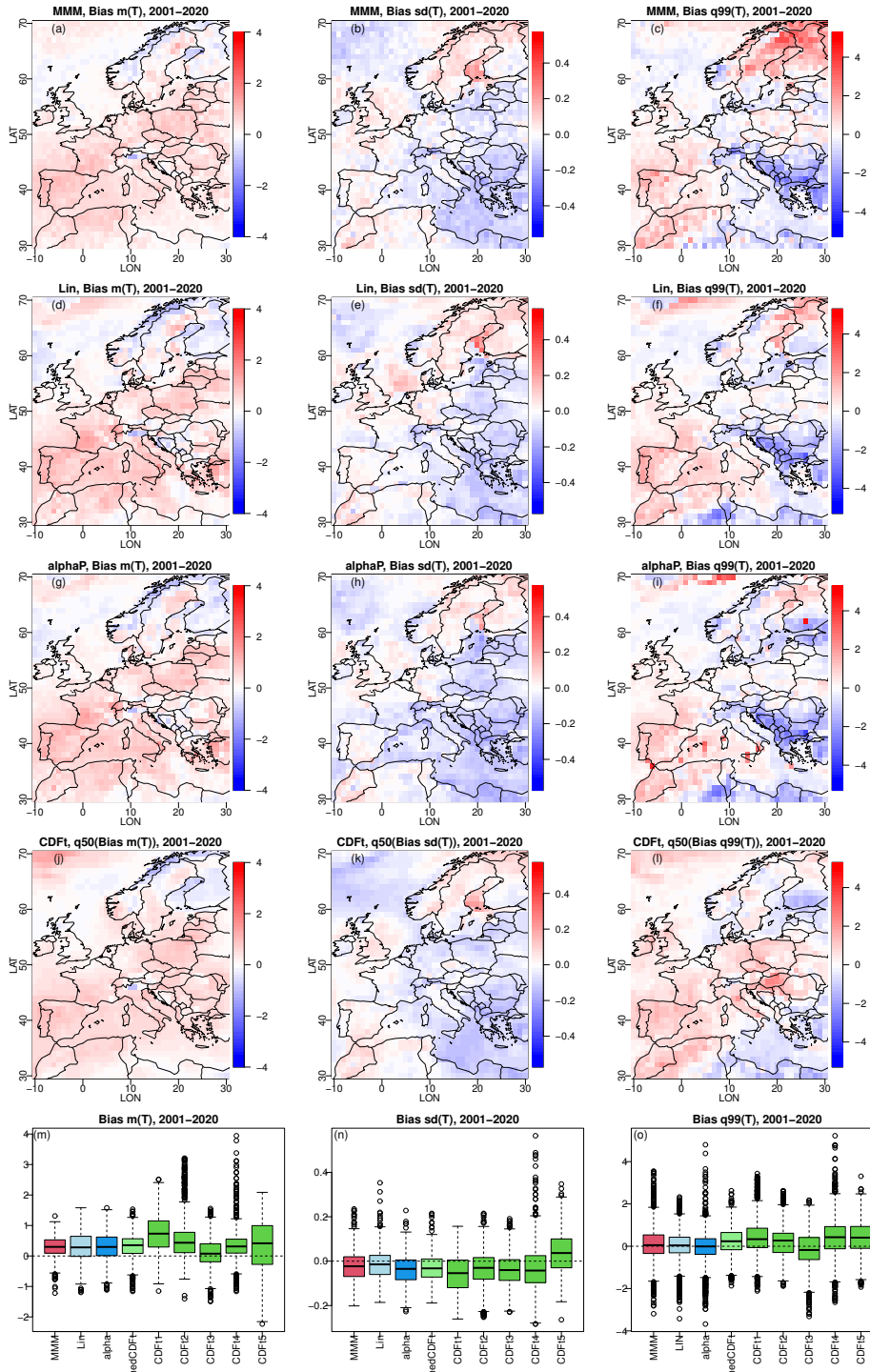


**Figure 5.** Biases in mean (left column), standard deviation (middle column) and 99% quantile (right column) for winter temperature from MMM (top row),  $\alpha$ -pooling (row 2), CDF-t (third row) and linear pooling (fourth row) under the 2001-2020 (projection) time period of the ERA5 experiment. Third row corresponds to the grid-point median of the CDF-t biases. Fifth (bottom) row: boxplots of biases for MMM, linear pooling,  $\alpha$ -pooling the median CDF-t biases, as well as for each of the 5 CDF-t results. The results for summer temperature are given as supplementary information in Figure S7.



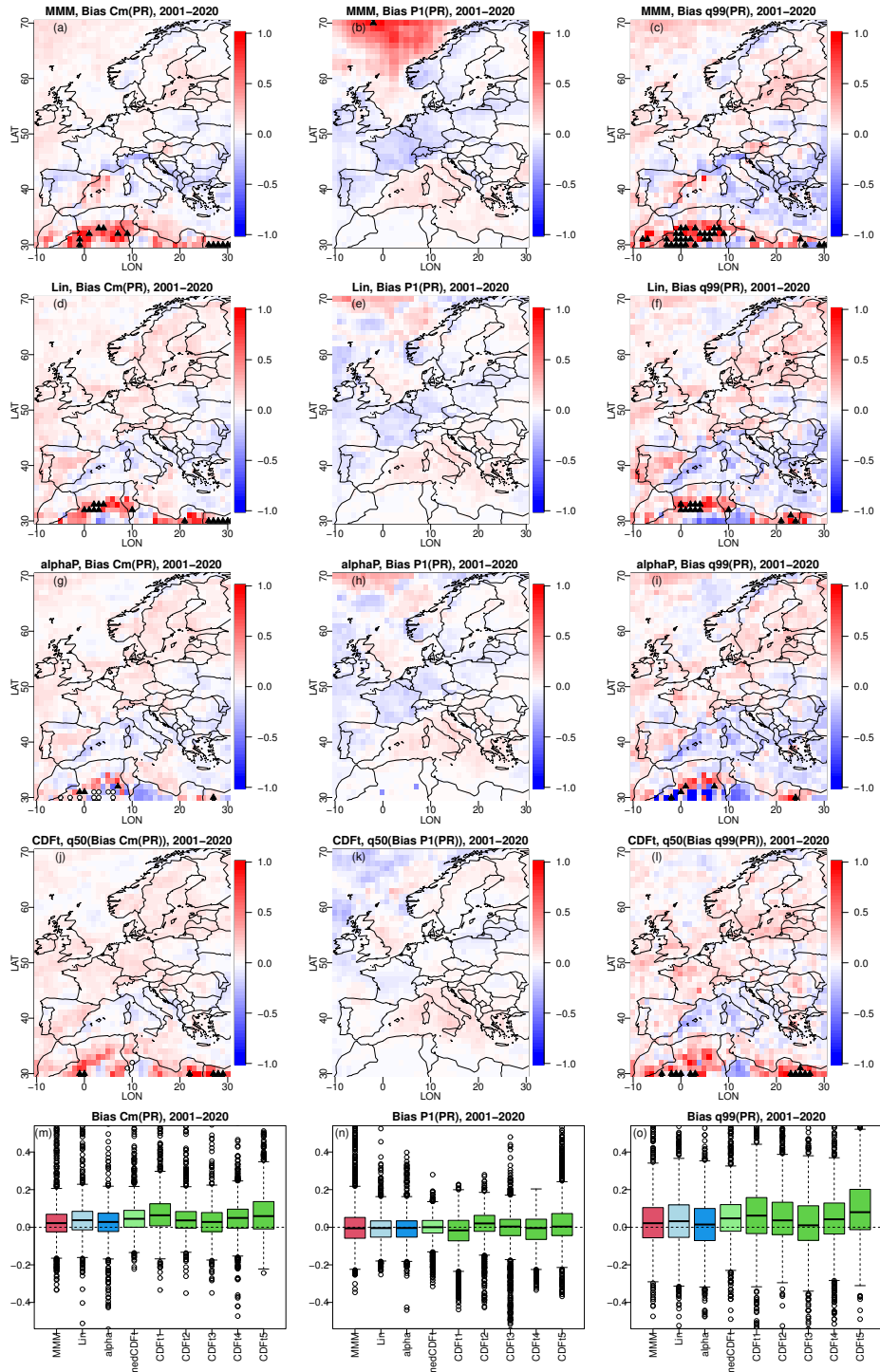


**Figure 6.** Same as Fig. 5 but for winter precipitation with biases in conditional mean given wet (left column), probability of dry day ( $P_1$ , middle column) and 99% quantile (right column). The results for summer are given as supplementary information in Figure S8.

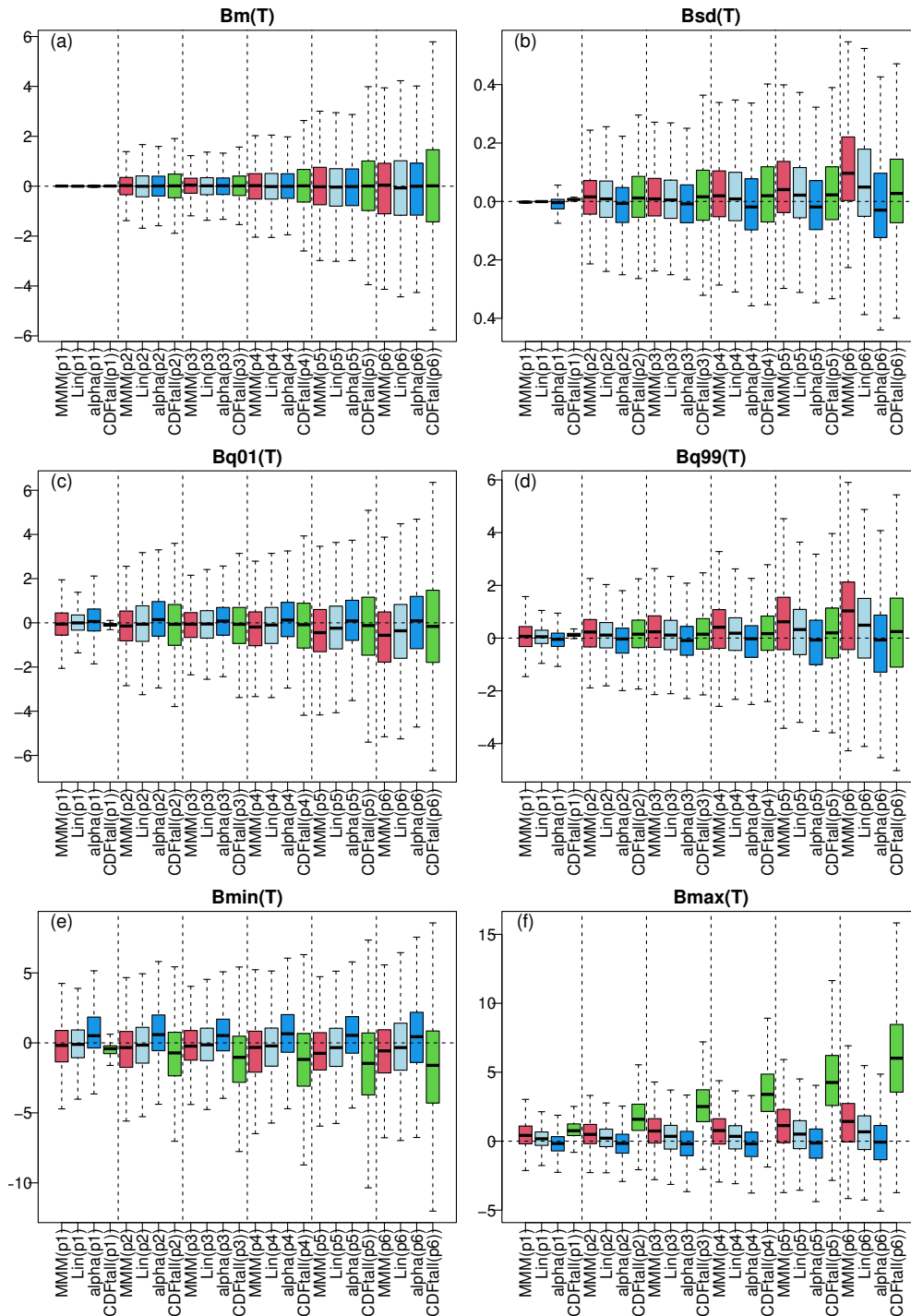


**Figure 7.** Results of the perfect model experiment for winter temperature: Boxplots of biases from the three methods (red=MMM, light blue=linear pooling, blue= $\alpha$ -pooling, green=CDF-t) for the six 20-year time periods (from p1=1981-2000=calibration to p6=2081-2100). The different panels display biases in (a) mean temperature, (b) standard deviation, (c) 1% quantile, (d) 99% quantile, (e) minimum and (f) maximum temperature. Note that, for CDF-t, the boxplots are drawn from the concatenation of all the individual CDF-t biases. Results for summer are provided as supplementary materials in Fig. S9.

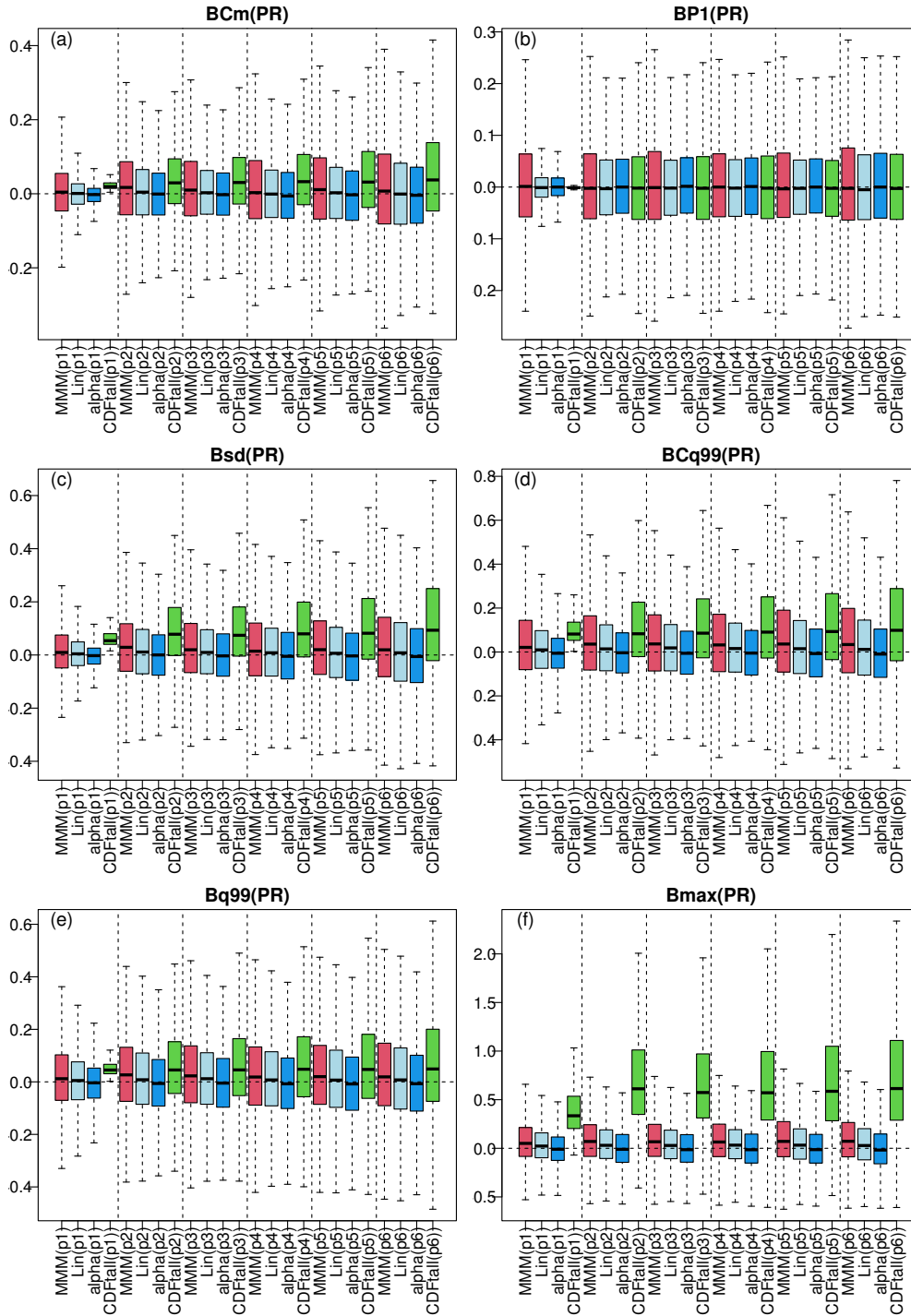


**Figure 8.** Results of the perfect model experiment for winter precipitation: Same as Fig. 7 but for precipitation. The different panels display biases in (a) conditional mean precipitation given wet, (b) probability of dry ( $< 1\text{mm}$ ) day, (c) standard deviation, (d) conditional 99% quantile given wet, (e) unconditional 99% quantile, and (f) maximum precipitation. Results for summer are provided as supplementary materials in Fig. S10.

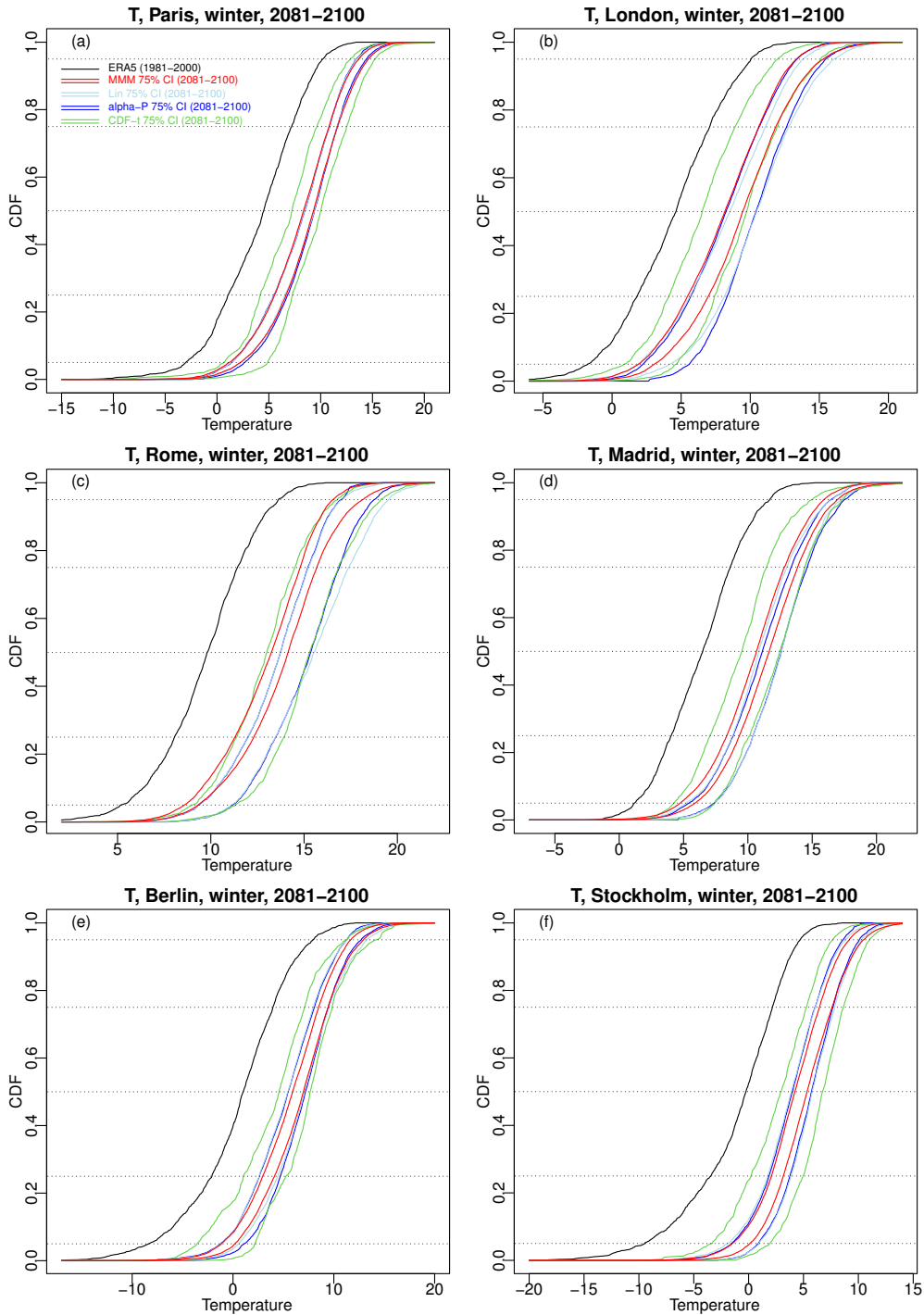


**Figure 9.** Results of the sensitivity experiment: For winter temperature over 2081-2100 and 6 major cities in western Europe, 75% confidence intervals for  $\alpha$ -pooling (blue lines), linear pooling (light blue lines), MMM (red lines) and CDFt (green lines). The temperature ERA5 CDF (black line) over 1981-2000 is also displayed for visual evaluation of changes. Results for summer are provided as supplementary material in Fig. S11.

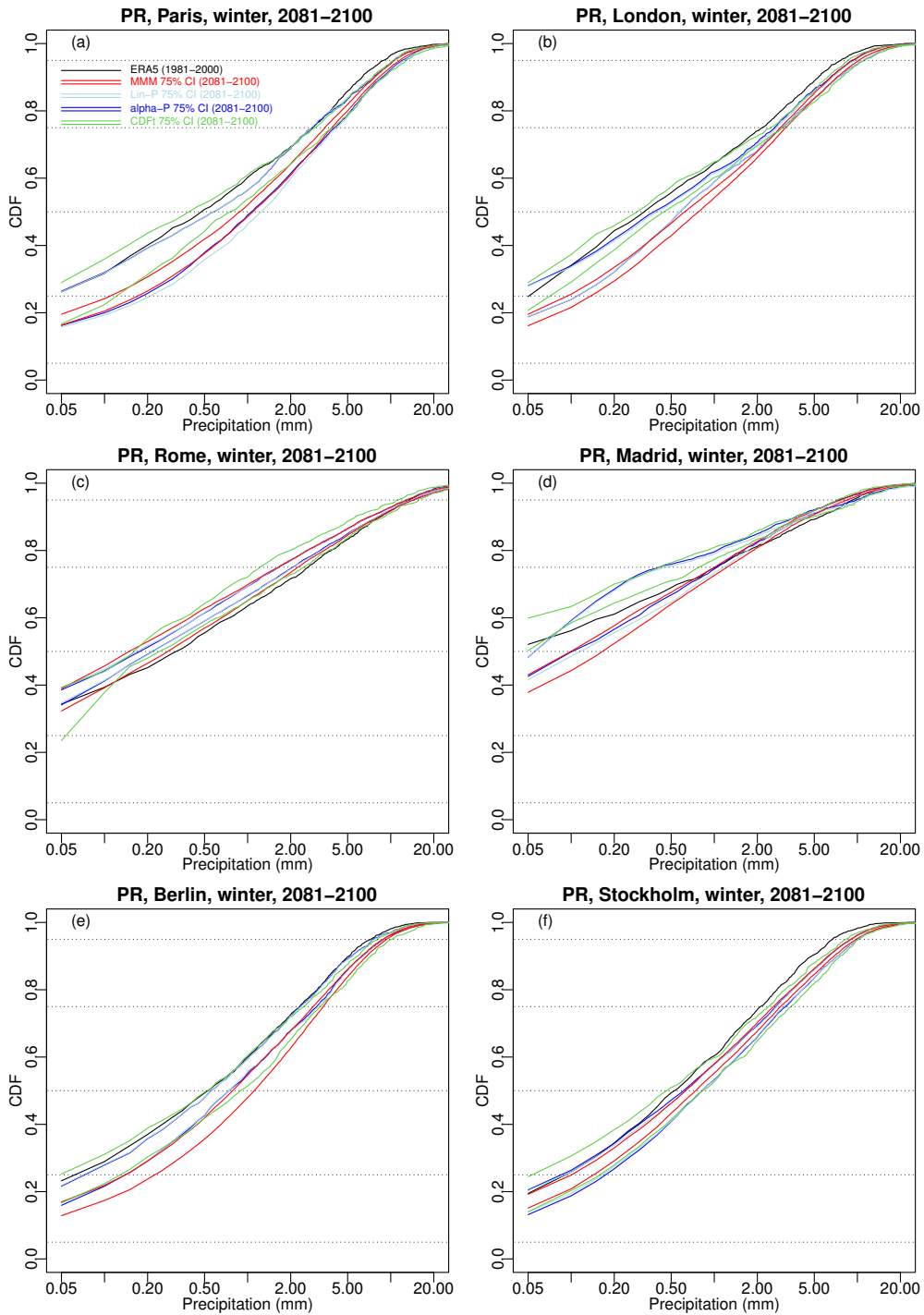


**Figure 10.** Results of the sensitivity experiment: Same as Fig. 9 but for precipitation. Note that the x-axis is displayed in log-scale to ease evaluation. Results for summer are provided as supplementary material in Fig. S12.

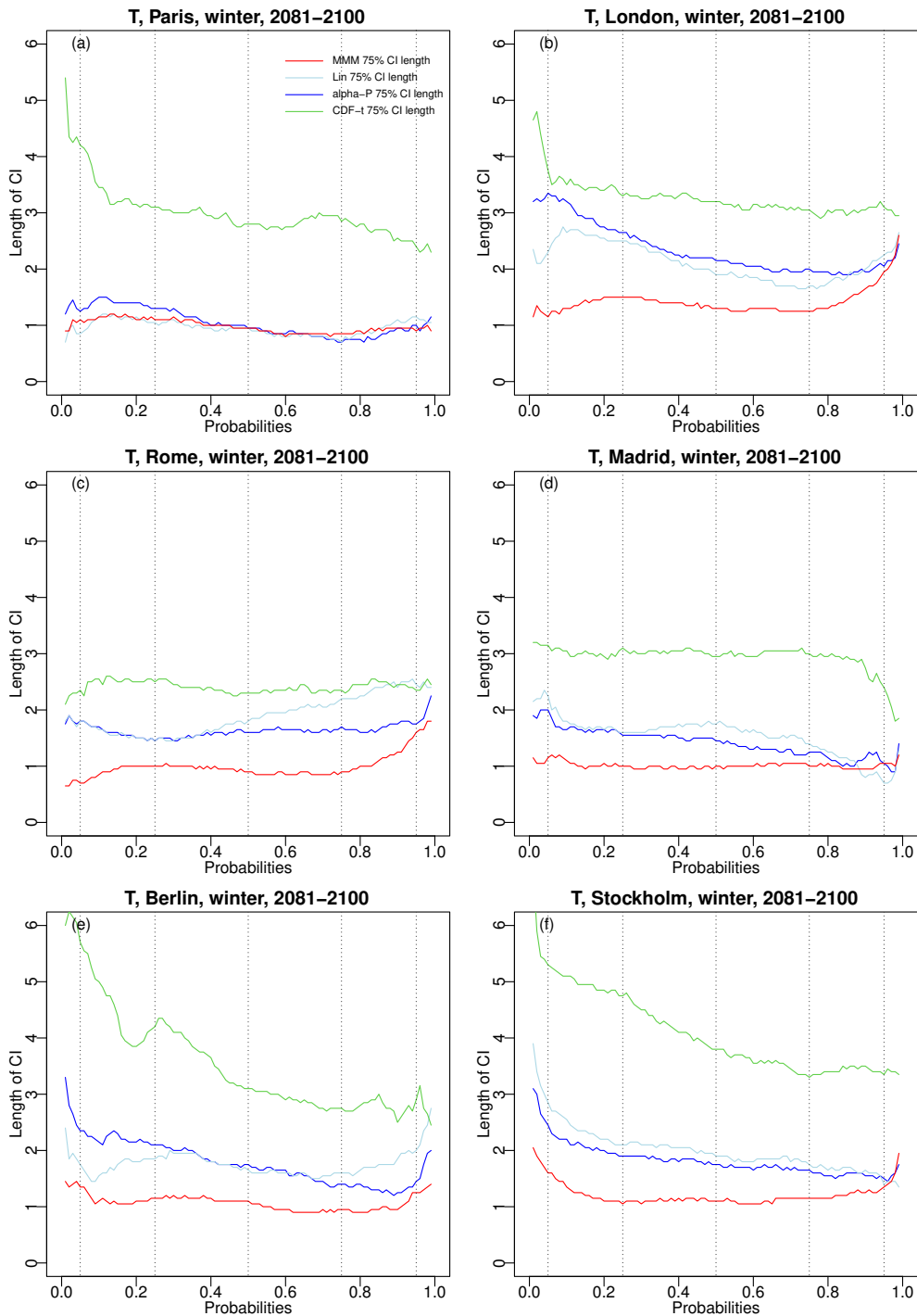


**Figure 11.** For winter temperature over 2081-2100 and 6 major cities in western Europe, width of the 75% CDF confidence intervals for MMM (red line), linear pooling (light blue line),  $\alpha$ -pooling (blue line), and CDFt (green line). Results for summer are provided as supplementary material in Fig. S13.

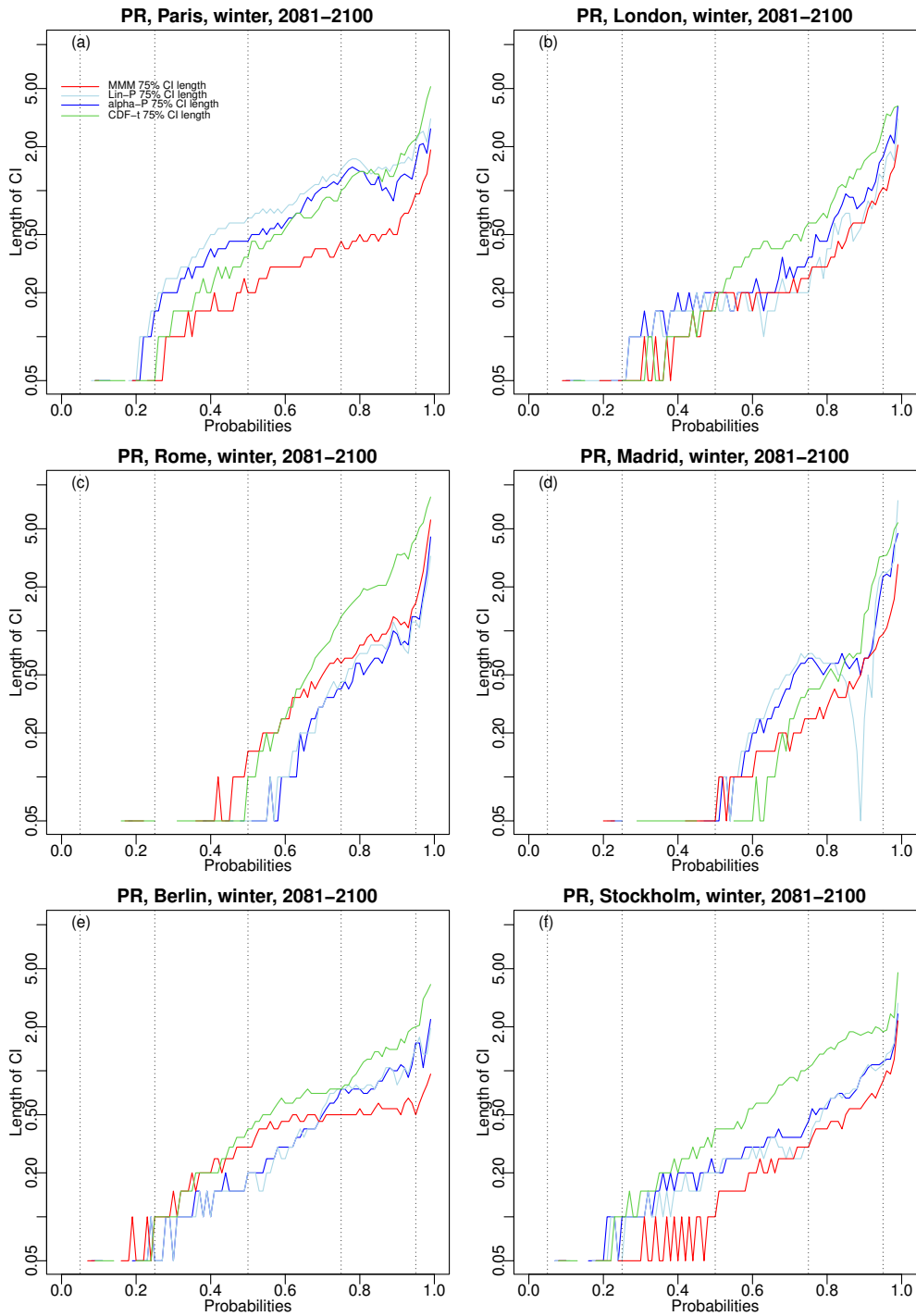


**Figure 12.** Same as Fig. 11 but for precipitation. Note that the y-axis is displayed in log-scale to ease evaluation. Results for summer are provided as supplementary material in Fig. S14.

## 820 Appendix A: An approximate solution to the $\alpha$ -Pooling

The well-known Box-Cox transformation  $B(F)(x) = (1 - F(x)^\alpha)/\alpha$ , with  $\alpha > 0$ , is well defined for all values  $F(x) \in [0, 1]$ , with  $\lim_{\alpha \rightarrow 0} B(F)(x) = -\ln F(x)$  when  $F(x) > 0$  and  $\lim_{\alpha \rightarrow 0} B(1 - F)(x) = -\ln(1 - F(x))$  when  $F(x) < 1$ . Let us consider a pooling approach that consists to assume that the Box-Cox transformation of the pooled CDF is, up to a normalizing factor  $K$ , the weighted average of the Box-Cox transformation, ie:

$$825 \quad B(K.F_B)(x) = \sum_{i=1}^N w_i B(F_i)(x), \quad \text{and} \quad B(K.(1 - F_B))(x) = \sum_{i=1}^N w_i B(1 - F_i)(x).$$

After multiplying by  $\alpha$  and rearranging, one gets

$$K^\alpha F_B(x)^\alpha = 1 + \sum_{i=1}^N w_i (F_i(x)^\alpha - 1) \quad \text{and} \quad K^\alpha (1 - F_B(x))^\alpha = 1 + \sum_{i=1}^N w_i (1 - F_i(x)^\alpha - 1).$$

From the fact that  $F_B(x) + 1 - F_B(x) = 1$ , one thus gets

$$830 \quad F_B(x) = \frac{[1 - S + \sum_{i=1}^N w_i F_i(x)^\alpha]^{1/\alpha}}{[1 - S + \sum_{i=1}^N w_i F_i(x)^\alpha]^{1/\alpha} + [1 - S + \sum_{i=1}^N w_i (1 - F_i(x)^\alpha)]^{1/\alpha}}, \quad \forall x \in \mathbb{R} \quad (\text{A1})$$

$$830 \quad \text{with } S = \sum_{i=1}^N w_i.$$

Let us now go back to the  $\alpha$ -pooling approach described in Section 3.4. Inspired by (A1), let us plug into the  $\alpha$ -pooling Equation (7) a solution of the form  $F_H(x)^\alpha = (\sum_{i=1}^N w_i F_i(x)^\alpha + A)/Z$  and  $(1 - F_H(x))^\alpha = (\sum_{i=1}^N w_i (1 - F_i(x)^\alpha) + A)/Z$ , where  $Z$  is a normalizing factor. From  $F_H(x) + 1 - F_H(x) = 1$  we find that  $Z^{1/\alpha} = [\sum_{i=1}^N w_i F_i(x)^\alpha + A]^{1/\alpha} + [\sum_{i=1}^N w_i (1 - F_i(x)^\alpha) + A]^{1/\alpha}$  and

$$835 \quad F_H(x) = \frac{[\sum_{i=1}^N w_i F_i(x)^\alpha + A]^{1/\alpha}}{[\sum_{i=1}^N w_i F_i(x)^\alpha + A]^{1/\alpha} + [\sum_{i=1}^N w_i (1 - F_i(x)^\alpha) + A]^{1/\alpha}},$$

which is nothing but (A1) with  $A = 1 - S$ . Hence  $F_H = F_B$ , and for the rest of this Section, we will use the notation  $F_B$  for both constructions.  $F_B$  is well defined for all  $\alpha > 0$  if  $S \leq 1$ . In this case, it can be shown that it is a non-decreasing function of  $x$  because its derivative with respect to  $x$  is non-negative. From

$$\lim_{x \rightarrow -\infty} F_B(x) = \frac{(1 - S)^{1/\alpha}}{(1 - S)^{1/\alpha} + 1} \quad \text{and} \quad \lim_{x \rightarrow \infty} F_B(x) = \frac{1}{(1 - S)^{1/\alpha} + 1}, \quad (\text{A2})$$

840 one finds that  $F_B$  in (A1) is a proper CDF if and only the condition  $S = 1$  is verified. In this case,  $F_B$  has the simpler expression

$$F_{B,1}(x) = \frac{[\sum_{i=1}^N w_i F_i(x)^\alpha]^{1/\alpha}}{[\sum_{i=1}^N w_i F_i(x)^\alpha]^{1/\alpha} + [\sum_{i=1}^N w_i (1 - F_i(x)^\alpha)]^{1/\alpha}}. \quad (\text{A3})$$

When  $\alpha = 1$ , the pooling formula (A3) reduces to the linear pooling. As  $\alpha \rightarrow 0$ , it is straightforward to check that it boils down to the log-linear pooling (4). As was the case for the  $\alpha$ -pooling presented in Section 3.4, this pooling formula generalizes thus



845 both the log-linear pooling and the linear pooling. It must be emphasized that replacing  $w_i$  by  $Kw_i$  with  $K > 0$  in (A3) leads to the same value  $F_{B,1}(x)$ . Imposing or not  $\sum_{i=1}^N w_i = 1$  in (A3) has thus no consequences on  $F_{B,1}$ .

The existence of two different pooling approaches, namely  $F_G$  and  $F_B$ , calls for some comments.

- On numerous tests, it was consistently found that the CDF  $F_G$  obtained by the  $\alpha$ -pooling (7) and the CDF  $F_{B,1}$  computed directly using (A3) are almost indistinguishable when imposing  $S = 1$ . In this case, the direct computation in (A3) is 5  
850 to 10 times faster and should be preferred.
- However, as discussed in Section 3.4,  $F_G$  is a proper CDF even if  $S > 1$ . There is thus an extra parameter available for the  $\alpha$ -pooling approach allowing for a better fit between the models and the reference. The cost to pay is increased computation time.
- When using the direct approach in (A1),  $S \leq 1$  leads to well defined values  $F_B(x)$ . It thus also offers an extra parameter  
855 for the pooling, but the CDF  $F_B$  varies between the limits in (A2) instead of  $[0, 1]$ . Strictly speaking,  $F_B$  is thus not a proper CDF. In practice however, it was very often found that the quantity  $((1 - S)^{1/\alpha} + 1)^{-1}$  was extremely small (say, less than  $10^{-3}$ ) and the "min-max" rescaling shown in Eq. (11) can be performed to get a proper CDF.
- In (A1)  $S > 1$  must be avoided as it can lead to inconsistent results, such as non monotonic functions  $F_B$ .

## Appendix B: Optimal properties of $\alpha$ -pooling

860 We report briefly some optimal properties of the  $\alpha$ -pooling presented in Section 3.4. We refer to Neyman and Roughgarden (2023) for a complete presentation on proper scoring rules, quasi-arithmetic pooling and min-max optimal properties. We first start with some generalities. For the sake of clarity,  $x$  is fixed and we write  $F$  for  $F(x)$ . We further define the vector  $\mathbf{F} = (F, 1 - F)^t$ . In what follows, vectors will be written in bold letters.

The accuracy of a pooling method for a probability distribution is assessed using a metric, called a scoring rule, which assigns a  
865 value (sometimes called a reward) when a probability  $q$  is reported and outcome  $j$  happens according to a reference probability  $\mathbf{p}$ . Among all possible scoring rules, we will restrict ourselves to *proper scoring rules*, i.e. a scoring rule that is maximized when the reported probability is  $q = \mathbf{p}$ . Well known examples of proper scoring rules are the Brier scoring rule (Brier et al., 1950) and the logarithmic scoring rule. As shown in Gneiting and Raftery (2007) and in Neyman and Roughgarden (2023, Theorem 3.1), proper scoring rules can be derived from a function  $G(\mathbf{p})$ , referred to as the *expected reward function*. According to this  
870 theorem a scoring rule is proper if and only if

$$s(\mathbf{p}; j) = G(\mathbf{p}) + \langle \mathbf{g}(\mathbf{p}), \delta_j - \mathbf{p} \rangle, \tag{B1}$$

where  $\mathbf{g}(\mathbf{p})$  is the gradient of  $G(\mathbf{p})$ . Let  $j = 1, \dots, J$  be the possible outcomes with probabilities  $\mathbf{p} = (p(1), \dots, p(J))$ . The Brier (also known as 'quadratic') scoring rule corresponds to  $G_{\text{Brier}}(\mathbf{p}) = \sum_j p(j)^2$  and the logarithmic scoring rule corresponds to  $G_{\log}(\mathbf{p}) = \sum_j p(j) \ln p(j)$ . A necessary condition on  $G$  is that it is a convex function with respect to  $\mathbf{p}$ . Neyman and

875 Roughgarden (2023) call *quasi-arithmetic pooling* any pooling formula defined by

$$\mathbf{g}(\mathbf{F}_G) = \sum_{i=1}^N w_i \mathbf{g}(\mathbf{F}_i), \quad w_i \geq 0, \quad i = 1, \dots, N, \quad \sum_{i=1}^N w_i = 1, \quad (\text{B2})$$

where  $g$  is the gradient of a proper scoring rule  $G$ . They showed (in Theorem 4.1) the following Max-Min property for *quasi-arithmetic pooling* formula. Let us defined the following utility function

$$u(\mathbf{F}; j) := s(\mathbf{F}; j) - \sum_{i=1}^N w_i s(\mathbf{F}_i; j) \quad (\text{B3})$$

880 which corresponds to the expected difference between the scoring rule applied to  $\mathbf{F}$  and the scoring rule applied to model  $i$ , chosen randomly according to  $\mathbf{w}$ . Then, the minimum  $\min_j u(\mathbf{p}; j)$  is maximized by setting  $\mathbf{F} = \mathbf{F}_G$  as given in (B6). In other words, the worst loss of scores (often interpreted as a reward) is maximized using quasi-arithmetic pooling.

In our case, for a given  $x$ , there are only two possible outcomes,  $j \in \{0, 1\}$ : being less than or equal to  $x$ , with probability  $p(0) = F$  and being above  $s$ , with probability  $p(1) = 1 - F$ . We now consider the following convex function

$$885 \quad G(\mathbf{F}) = F^{1+\alpha} + (1 - F)^{1+\alpha}, \quad (\text{B4})$$

with the limit case  $\lim_{\alpha \rightarrow 0} G(\mathbf{F}) = F \ln F + (1 - F) \ln(1 - F)$  corresponding to the logarithmic scoring rule. Notice that  $\alpha = 1$  corresponds to the Brier scoring rule. The associated gradient is

$$\mathbf{g}(\mathbf{F}) = (1 + \alpha)(F^\alpha, (1 - F)^\alpha)^t, \quad (\text{B5})$$

with  $\lim_{\alpha \rightarrow 0} \mathbf{g}(\mathbf{F}) = (1 + \ln F, 1 + \ln(1 - F))^t$ . Since in (B4) the function  $G$  is convex, the scoring rule given by (B1) is  
 890 proper and each component of the gradient is a continuous and injective function of  $F$ , for all values  $\alpha \geq 0$ . The scoring rule associated to  $G(\mathbf{F})$  in (B4) varies thus continuously from the logarithmic scoring rule to the Brier scoring rule as  $\alpha$  varies from 0 to 1. Notice that  $\alpha$  is also allowed to be larger than 1, but the scoring rule has no specific name in that case. The pooling formula defined by

$$\mathbf{H}_2 \mathbf{g}(\mathbf{F}_G) = \sum_{i=1}^N w_i \mathbf{H}_2 \mathbf{g}(\mathbf{F}_i), \quad w_i \geq 0, \quad i = 1, \dots, N, \quad \sum_{i=1}^N w_i = 1, \quad (\text{B6})$$

895 where  $\mathbf{H}_2$  is the (1,2) Helmert matrix, corresponds exactly to the  $\alpha$ -pooling presented in Section 3.4, which thus inherits the optimal properties of quasi arithmetic pooling.